Electronic Supplementary Material (ESI) for Journal of Materials Chemistry A.
This journal is © The Royal Society of Chemistry 2019

Electronic Supplementary Information

Conversion pseudocapacitance-contributing and robust hetero-nanostructural perovskite $KCo_{0.54}Mn_{0.46}F_3$ nanocrystals anchored on graphene nanosheets anodes for advanced lithium-ion capacitor, battery and their hybrids

Danfeng Ying,[a] Rui Ding,[a] Yongfa Huang,[a] Wei Shi,[a] Qilei Xu,[a] Caini Tan,[a] Xiujuan Sun,[a] Ping Gao [a] and Enhui Liu [a]*

[a]Key Laboratory of Environmentally Friendly Chemistry and Applications of Ministry of Education, College of Chemistry, Xiangtan University, Xiangtan, Hunan 411105, P.R. China

*E-mails: drm8122@163.com; drm8122@xtu.edu.cn

Table of contents		
Experimental section	Synthesis of materials, characterizations, electrochemical measurements and methods: calculations for m_+/m_-, C_m, E_m, P_m.	P 4
Figure S1.	The crystalline structures of perovskite KMF_3 (a) and crystalline parameters for $KCoF_3$ and $KMnF_3$ (b).	P 6
Figure S2.	A picture of representative KCMF (Co/Mn=1:0, 3:2, 0:1), U-KCMF(3:2)/rGO and KCMF(3:2)/rGO samples.	P 6
Figure S3.	SEM (a, b) and TEM (c, d) images of KCMF(3:2) sample.	P 7
Figure S4.	EDS and mapping of KCMF(3:2) sample with a scale barof 5 μm.	P 7
Figure S5.	EDS and mapping of KCMF(3:2) sample with a a scale bar of 700 nm.	P 8
Figure S6.	SEM (a, b), TEM (c) and HRTEM (d) images of U-KCMF(3:2)/rGO sample.	P 9
Figure S7.	EDS and mapping of U-KCMF(3:2)/rGO sample with a scale bar of 1 μm.	P 9
Figure S8.	SEM (a, b) and TEM (c, d) images of KCMF(3:2)/rGO sample.	P 10
Figure S9.	EDS and mapping of KCMF(3:2)/rGO sample with a scale bar of 600 nm.	P 10
Figure S10.	RS of U-KCMF(3:2)/rGO and KCMF(3:2)/rGO samples (a) and TG of KCMF(3:2), U-KCMF(3:2)/rGO and KCMF(3:2)/rGO samples (b).	P 11
Figure S11.	CV plots for the first three cycles of KCMF(6:1), (3:1), (1:1), (2:3), (1:3) and (1:6) electrodes at 0.3 mV s^{-1}.	P 12
Figure S12.	GCD curves for the first five cycles of KCMF (Co/Mn=1:0~0:1) electrodes at 0.1 A g^{-1}.	P 12
Figure S13.	GCD curves for the respective 3rd cycles at 3.2~0.1 A g^{-1} of KCMF (Co/Mn=1:0~0:1) electrodes.	P 13
Figure S14.	Rate performance and coulombic efficiency of KCMF (Co/Mn=1:0~0:1) electrodes at 0.1~3.2~0.1 A g^{-1}.	P 14
Figure S15.	Cycling stability and coulombic efficiency of KCMF (Co/Mn=1:0~0:1) electrodes at 2 A g^{-1} for 1000 cycles.	P 15
Figure S16.	Electrochemical performance of U-KCMF(3:2)/rGO and KCMF(3:2)/rGO electrodes.	P 16
Figure S17.	The equivalent circuits used to fit the experimental Nyquist plots before (a) and after (b) cycling of KCMF(3:2), U-KCMF(3:2)/rGO and KCMF(3:2)/rGO electrodes.	P 16
Figure S18.	CV plots for the first three cycles of KCMF(1:0) and (0:1) electrodes at 0.3 mV s^{-1}.	P 17
Figure S19.	The comparison of CV plots for the 3rd cycle at 0.1 and 0.3 mV s^{-1} of KCMF(1:0) (a), (0:1) (b), (3:2) (c) U-KCMF(3:2)/rGO (d) and KCMF(3:2)/rGO (e) electrodes.	P 17
Figure S20.	EDS (a), and mapping (b-g) for the KCMF(3:2) electrode discharged-0.01V state of the first GCD (0.05 A g^{-1}) cycle.	P 18
Figure S21.	EDS (a), and mapping (b-g) for the KCMF(3:2) electrode charged-3.0V state of the first GCD (0.05 A g^{-1}) cycle.	P 19
Figure S22.	Schematics of reaction mechanisms for KCMF(3:2) electrode during the discharging/charging processes under the first two cycles (a); Crystalline structure information of Co, Mn, CoF_2, MnF_2, LiF, KF and Li_2CO_3 phases (b).	P 20
Figure S23.	Electrochemical performance of AC electrode.	P 21
Figure S24.	Electrochemical performance of LFP electrode.	P 21
Figure S25.	The comparisons of electrochemical performance between AC/LFP(3:1), (1:1) and (1:3) electrodes.	P 22
Figure S26.	Electrochemical performance of AC/LFP(3:1) electrode.	P 22
Figure S27.	Electrochemical performance of AC/LFP(1:1) electrode.	P 23
Figure S28.	Electrochemical performance of AC/LFP(1:3) electrode.	P 23
Figure S29.	CV windows at 30 mV s^{-1} of these nine kinds of lithium-ion energy storage devices.	P 24

Experimental section

Synthesis of materials

The chemicals and reagents used in this paper are of analytical level (A.R.) and are used without further treatment (**Table S1**). A facile one-pot solvothermal method is applied to synthesize these perovskite fluorides. As all the synthetic steps of KCMF are the same except for the usage amounts of cobalt and manganese salts, the synthetic procedure of KCMF(3:2) is taken out as an example: i) Dissolve 1.2 mmol $CoCl_2·6H_2O$, 0.8 mmol $MnCl_2·4H_2O$, 5 mmol $KF·2H_2O$ and 0.2 g PVP-K30 into 35 mL solvents of ethylene glycol (EG); ii) Magnetically stir the mixture thoroughly and disperse it in an ultrasonic bath at 100 W for 30 minutes; iii) transfer the mixture into a 50 mL Teflon-lined stainless steel autoclave, heat it at 180°C for 12 h in an electric oven, then cool down naturally; iv) Centrifuge the yielded precipitates with absolute alcohol for several times to wash the product; v) Dry it at 95 °C for 12 h to obtain the final product. The synthesis procedure of U-KCMF(3:2)/rGO is the same as KCMF(3:2), except that 50 mg graphene oxides (GO) are dispersed in 35mL EG with the ultrasonic treatment for 3 h before the raw materials adding into the solvents. The KCMF(3:2)/rGO sample is obtained by ball-milling the U-KCMF(3:2)/rGO powder under the condition of 1500 rpm for 1 h.

Characterizations

The phases and crystallinity properties are determined by X-ray diffraction (XRD). The surface chemical compositions and electronic structures are checked by X-ray photoelectron spectra (XPS). The morphology and size of particles are analyzed by scanning electron microscopy (SEM) and transmission electron microscopy (TEM). The crystalline microstructures are resolved by the high-resolution TEM (HRTEM) and selected area electron diffraction (SAED). The element composition and distribution are measured by inductively coupled plasma-optical emission spectrometer (ICP-OES), X-Ray energy dispersive spectra (EDS) and mapping. The specific surface area, pore volume and size distribution are examined by nitrogen isothermal sorptions with Brunauer-Emmett-Teller (BET) and Barrett-Joyner-Halenda (BJH) methods. The existence and content of reduction graphene oxide are analyzed by Raman spectrum (RS) and Thermogravimetric analysis (TG).

Electrochemical measurements

The following is the procedure of preparing electrodes: i) Mix 70 wt.% active materials (as-synthesized KCMF, U-KCMF(3:2)/rGO, KCMF(3:2)/rGO or commercial AC, LFP, AC/LFP (3:1, 1:1, 1:3 in weight)), 20 wt.% conductive agent of acetylene black (AB) and 10 wt.% binder of polyvinylidene fluoride (PVDF) evenly with N-methyl-2-pyrrolidone (NMP)); ii) Caste the mixture onto Cu foil and carbon-coated Al foil used for the current collector of anodes and cathodes respectively; iii) Dry them in a vacuum oven at 110 °C for 12 h; iv) Cut them into disks with diameter of 12 mm with the active materials mass loading of about 1.2-5 mg cm^{-2}. In this paper, half-cells are fabricated using the 2032 coin cells with active materials as working electrodes, a Li plate as both counter and reference electrodes, glass fiber as separator and 1 M $LiPF_6$ dissolving in the mixed solvents of ethylene carbonate (EC), ethyl methyl carbonate (EMC) and dimethyl carbonate (DMC) (1:1:1 in volume) with 1% vinylene carbonate (VC) additives (LBC-305-01, CAPCHEM) as electrolyte to test the performance of materials. Tests for the different energy storage devices (LICs, LIBs, LIC/Bs) are conducted via full-cells with certain mass ratios of anode and cathode active materials (**Table S6**). All cell assemblies are performed in a high pure Ar-filled dry glovebox (MIKROUNA, O_2 and H_2O<0.1 ppm) and all tests are carried out at room temperature (about 25 ℃) except the assigned tests under high (40 ℃) and low (-20 ℃) temperatures. (The more detailed information of the above-mentioned material, chemicals and reagents can be seen in **Table S1**)

Methods: calculations for m_+/m_-, C_m, E_m, P_m

The charge-balance (Q+=Q-) as shown in equation S(1) is used to calculated the mass ratios of cathodes and anodes materials. The specific capacity (C_m, mAh g^{-1}), energy density ($E_{m,1}$, Wh kg^{-1}) for LICs, energy density ($E_{m,2}$, Wh kg^{-1}) for LIBs and LIC/Bs, and power density (P_m, kW kg^{-1}) of the different energy storage devices are calculated according to the equations S(2), S(3), S(4) and S(5).

$$m_+/m_- = Q_{m-}/Q_{m+} \qquad \text{S(1)}$$

$$C_m = Q_m/3.6 = It/3.6m \qquad \text{S(2)}$$

$$E_{m,1} = (C_m \triangle V)/2 \qquad \text{S(3)}$$

$$E_{m,2} = (C_m V) \qquad \text{S(4)}$$

$$P_m = 3.6E_m/t_d \qquad \text{S(5)}$$

Where m, Q_m, $\triangle V$, V, I and t refer to the mass of active materials (g, for half cells, it means the mass of active materials of anode or cathode; for full-cells, it means the total masses of active materials of anode and cathode), specific charge or discharge quantity (C g^{-1}, for anode, it means the charge quantity; for cathode and full-cells, it refers to the discharge quantity), potential window (V), potential of the discharging plateaus (V), current (A) and discharging time (s), respectively.

Supplemental figures

(a)

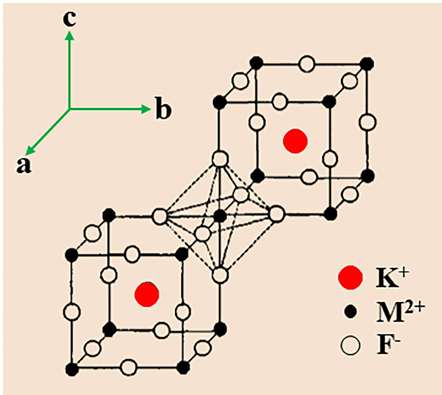

(b)

Sample	ICDD-PDF	Crystal system	Space group	Cell (a×b×c)/Å^3
$KCoF_3$	18-1006	Cubic	Pm-3m	4.0708×4.0708×4.0708
$KMnF_3$	17-0116	Cubic	Pm-3m	4.1890×4.1890×4.1890

Figure S1. The crystalline structures of perovskite KMF_3 (a) and crystalline parameters for $KCoF_3$ and $KMnF_3$ (b).

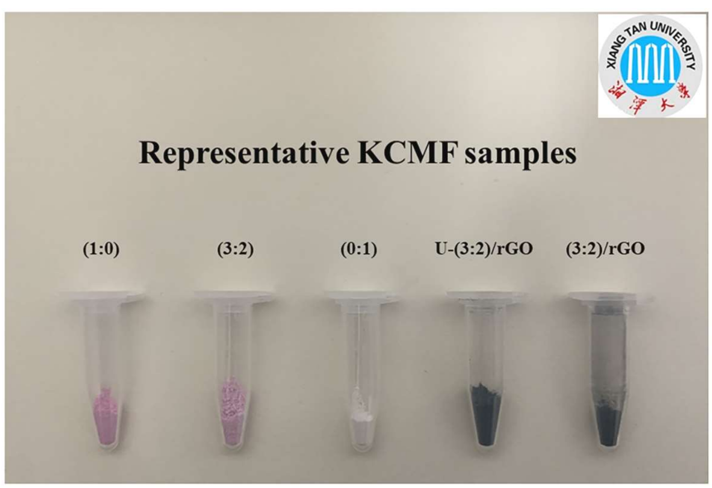

Figure S2. A picture of representative KCMF (Co/Mn=1:0, 3:2, 0:1), U-KCMF(3:2)/rGO and KCMF(3:2)/rGO samples.

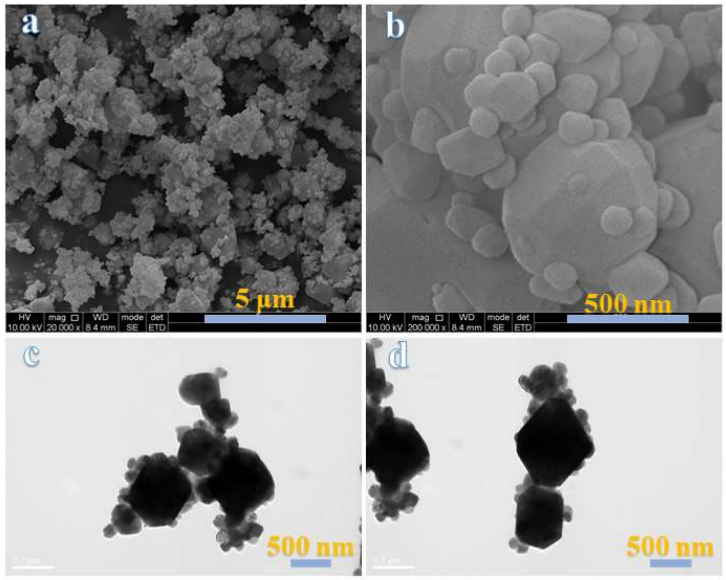

Figure S3. SEM (a, b) and TEM (c, d) images of KCMF(3:2) sample.

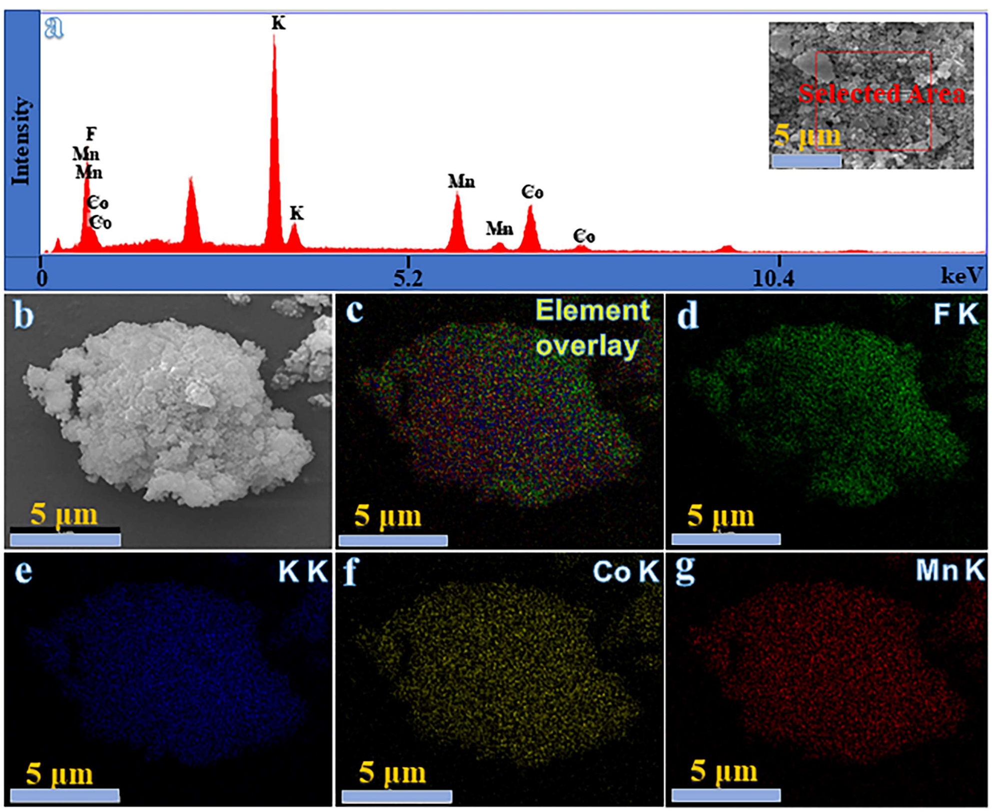

Figure S4. EDS and mapping of KCMF(3:2) sample with a scale bar of 5 μm.

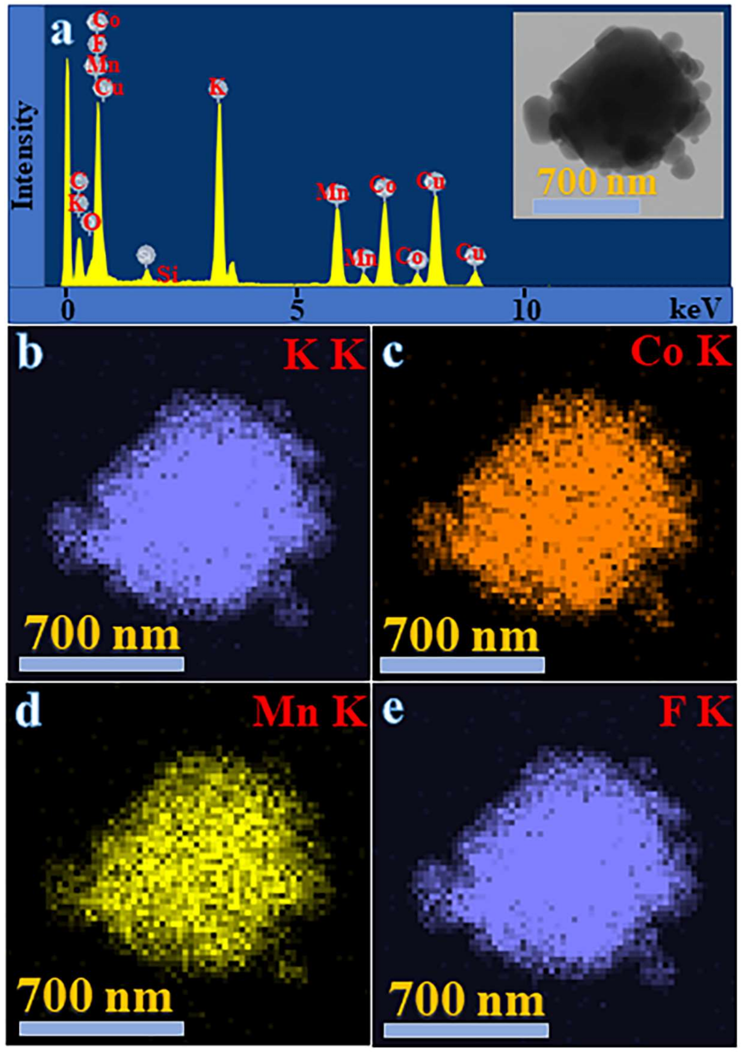

Figure S5. EDS and mapping of KCMF(3:2) sample with a scale bar of 700 nm.

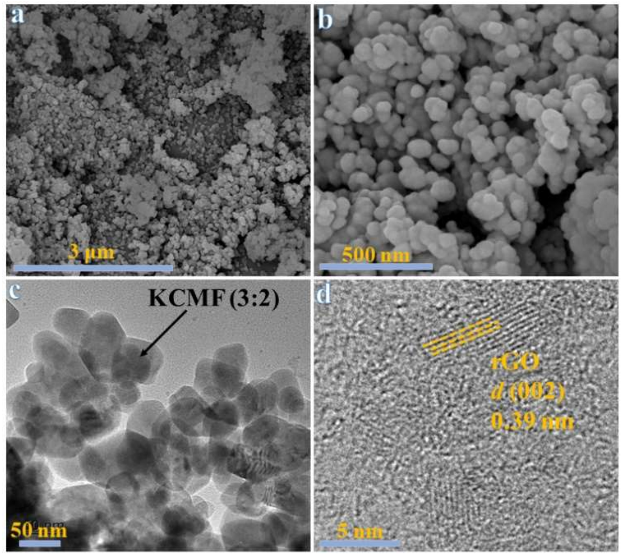

Figure S6. SEM (a, b), TEM (c) and HRTEM (d) images of U-KCMF(3:2)/rGO sample.

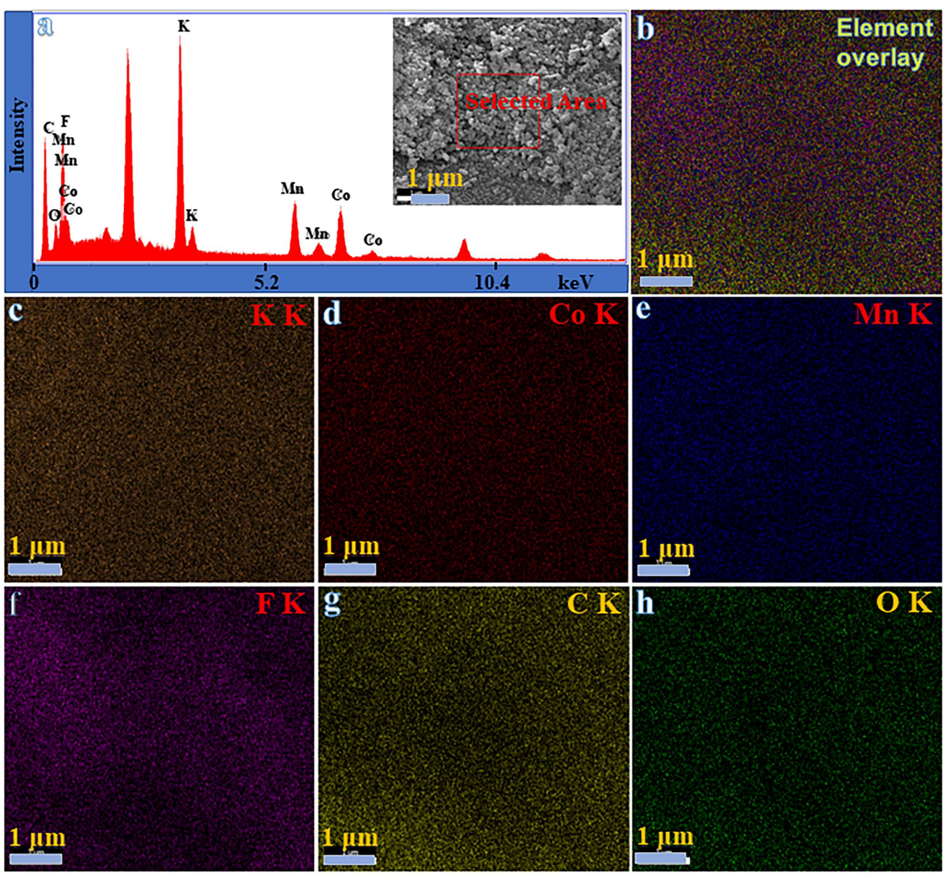

Figure S7. EDS and mapping of U-KCMF(3:2)/rGO sample with a scale bar of 1 μm.

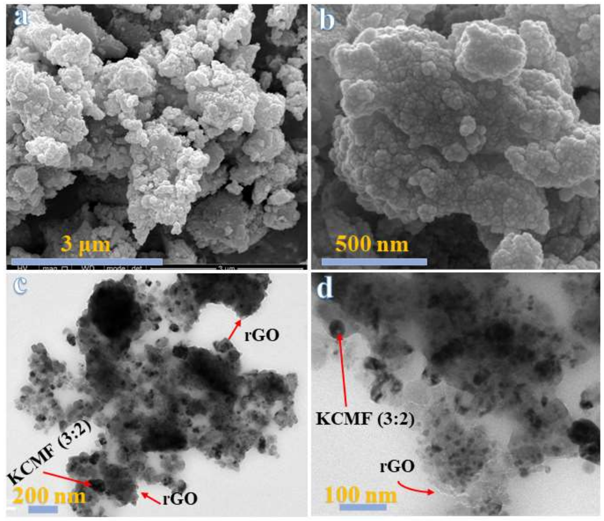

Figure S8. SEM (a, b) and TEM (c, d) images of KCMF(3:2)/rGO sample.

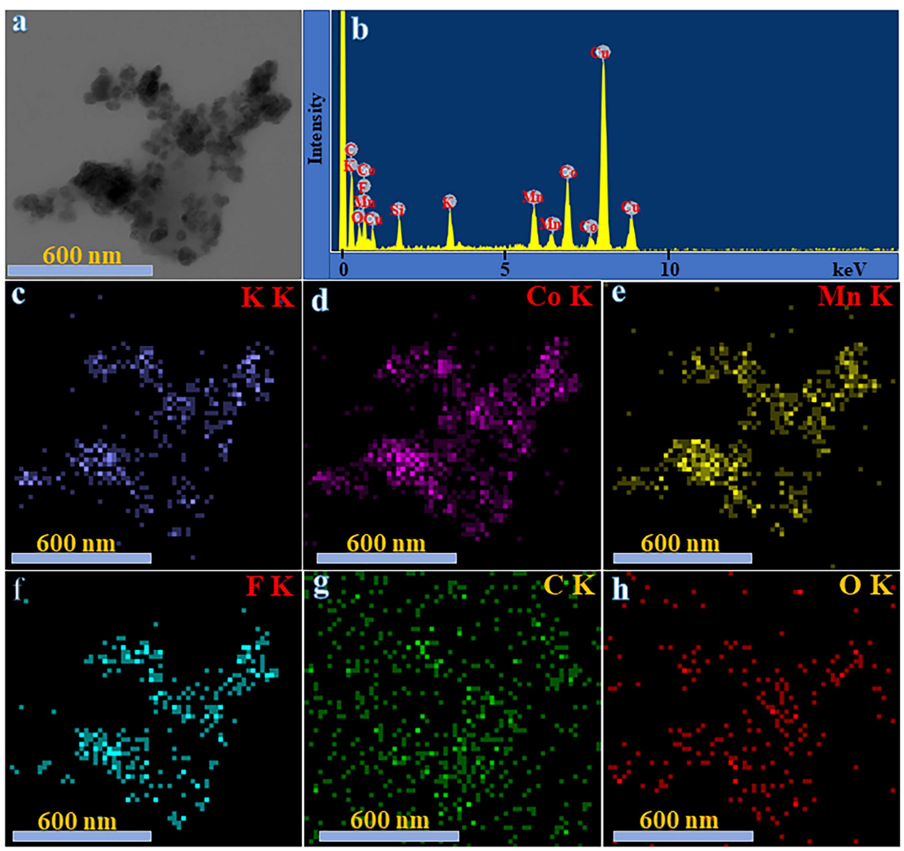

Figure S9. EDS and mapping of KCMF(3:2)/rGO sample with a scale bar of 600 nm.

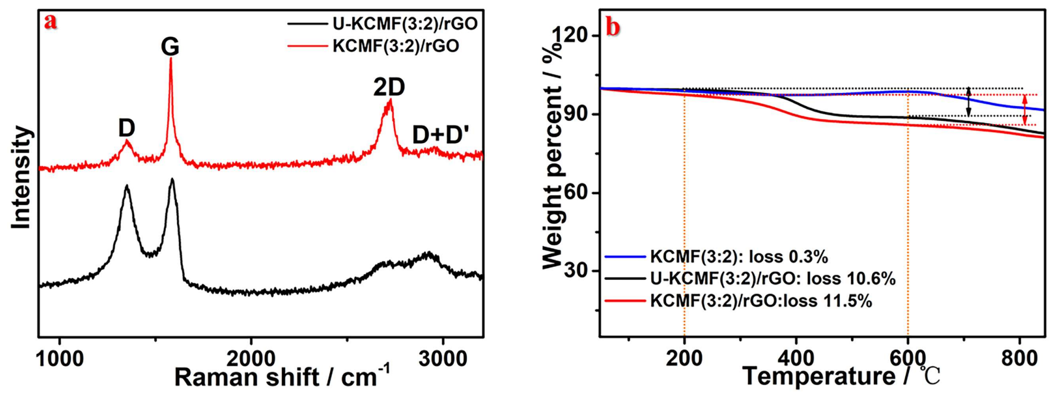

Figure S10. RS of U-KCMF(3:2)/rGO and KCMF(3:2)/rGO samples (a) and TG of KCMF(3:2), U-KCMF(3:2)/rGO and KCMF(3:2)/rGO samples (b).

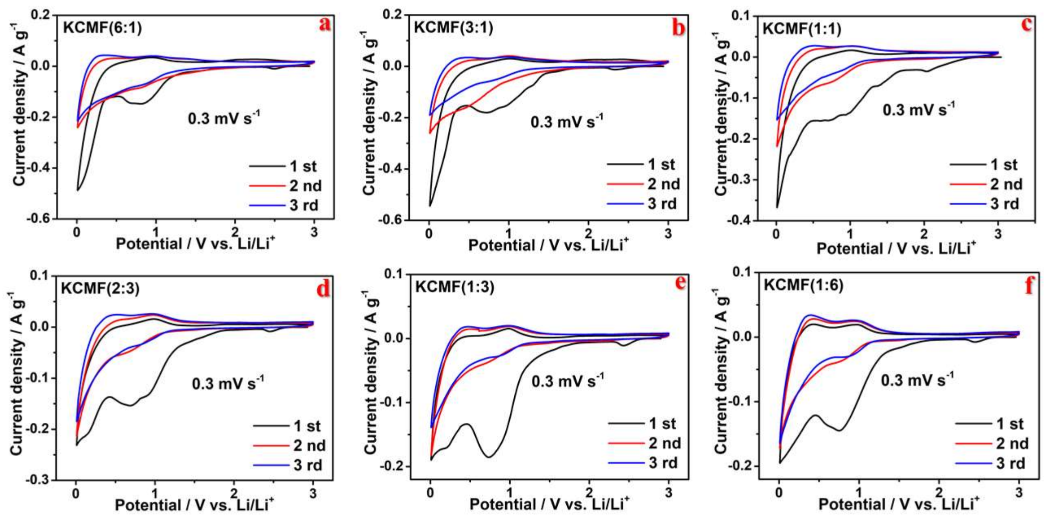

Figure S11. CV plots for the first three cycles of KCMF (6:1), (3:1), (1:1), (2:3), (1:3) and (1:6) electrodes at 0.3 mV s^{-1}.

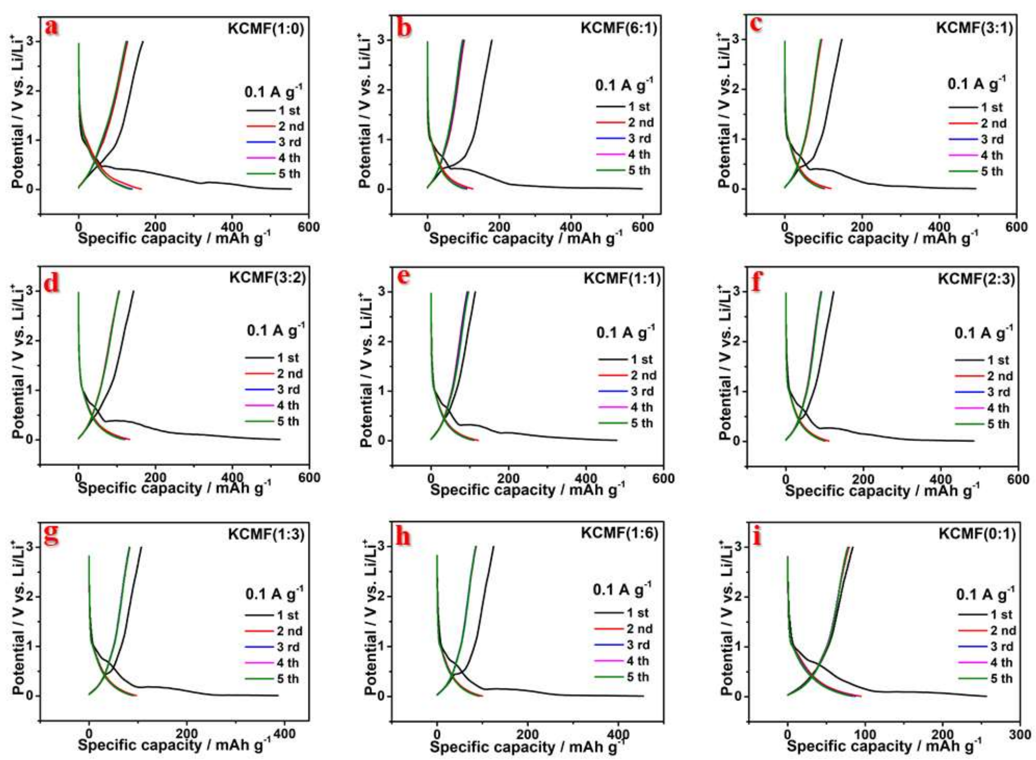

Figure S12. GCD curves for the first five cycles of KCMF (Co/Mn=1:0~0:1) electrodes at 0.1 A g^{-1}.

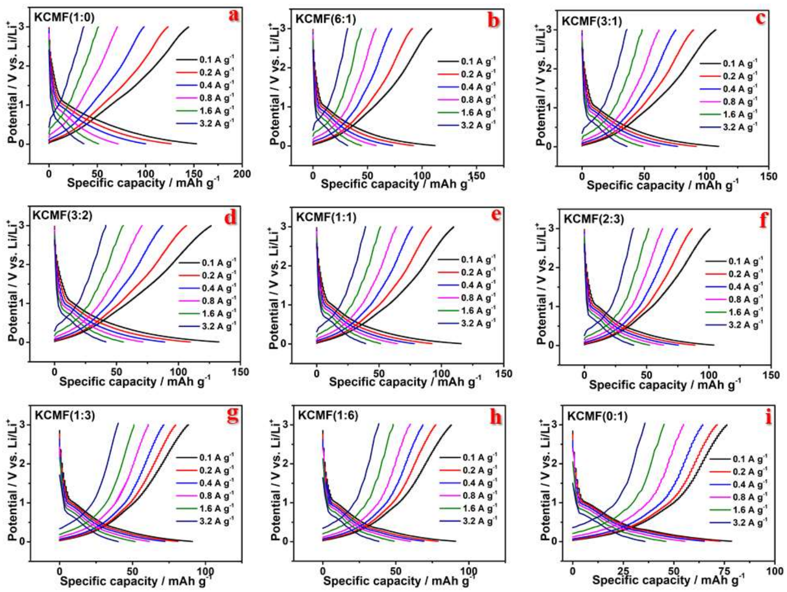

Figure S13. GCD curves for the respective 3rd cycles at 3.2~0.1 A g^{-1} of KCMF (Co/Mn=1:0~0:1) electrodes.

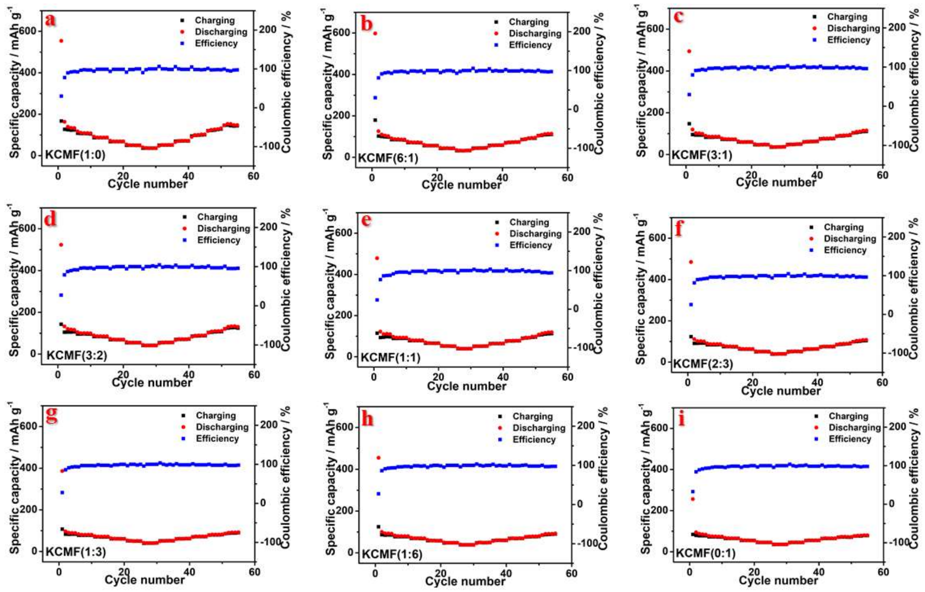

Figure S14. Rate performance and coulombic efficiency of KCMF (Co/Mn=1:0~0:1) electrodes at 0.1~3.2~0.1 A g^{-1}.

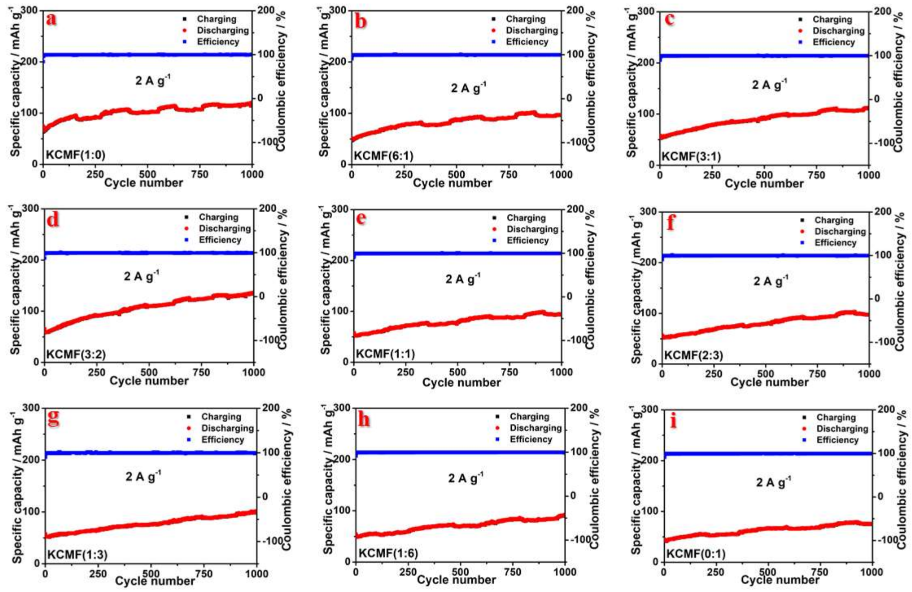

Figure S15. Cycling stability and coulombic efficiency of KCMF (Co/Mn=1:0~0:1) electrodes at 2 A g^{-1} for 1000 cycles.

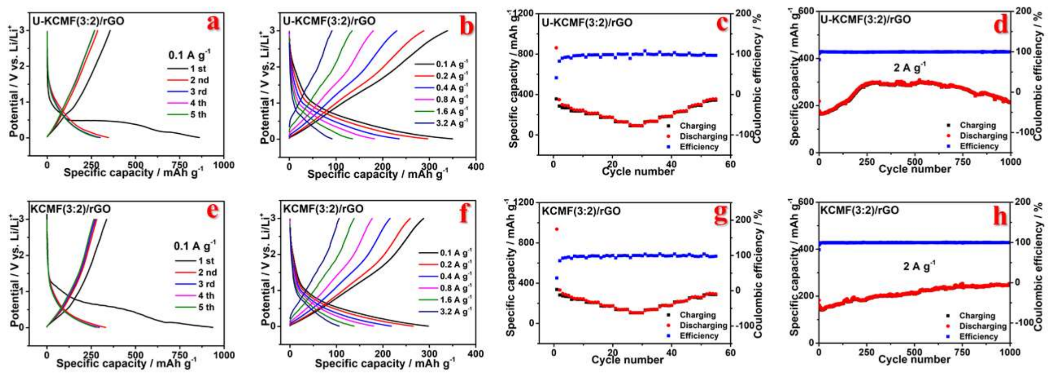

Figure S16. GCD curves for the first five cycles at 0.1 A g^{-1} (a, e), GCD curves for the respective 3rd cycle at 3.2~0.1 A g^{-1} (b, f), rate performance and coulombic efficiency at 0.1~3.2~0.1 A g^{-1} (c, g), and cycling stability and coulombic efficiency at 2 A g^{-1} for 1000 cycles (d, h) of U-KCMF(3:2)/rGO and KCMF(3:2)/rGO electrodes.

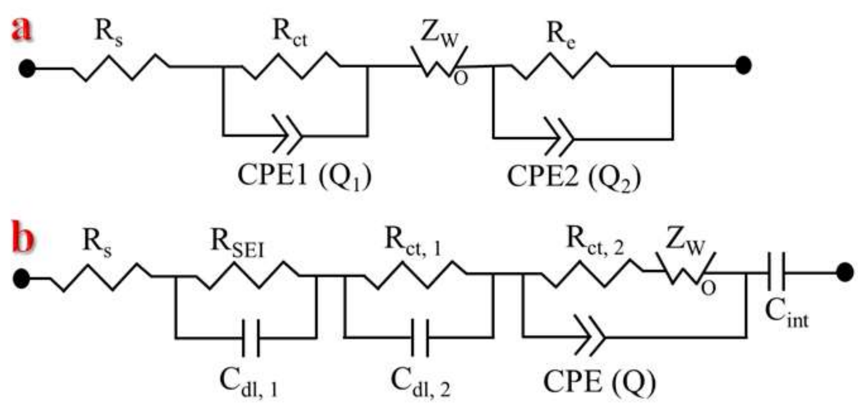

Figure S17. The equivalent circuits used to fit the experimental Nyquist plots before (a) and after (b) cycling of KCMF(3:2), U-KCMF(3:2)/rGO and KCMF(3:2)/rGO electrodes.

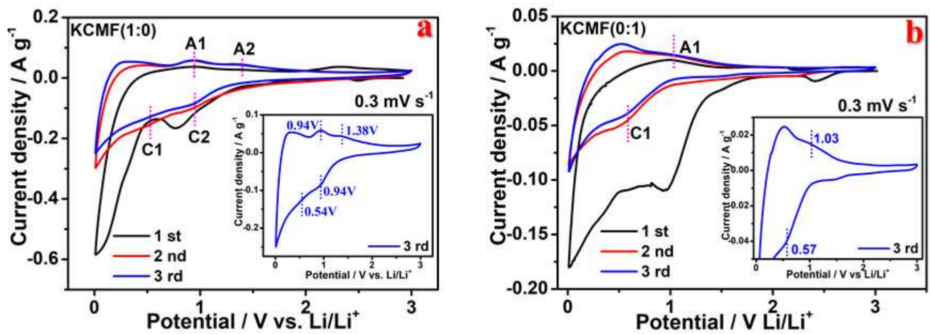

Figure S18. CV plots for the first three cycles of KCMF(1:0) and (0:1) electrodes at 0.3 mV s^{-1}.

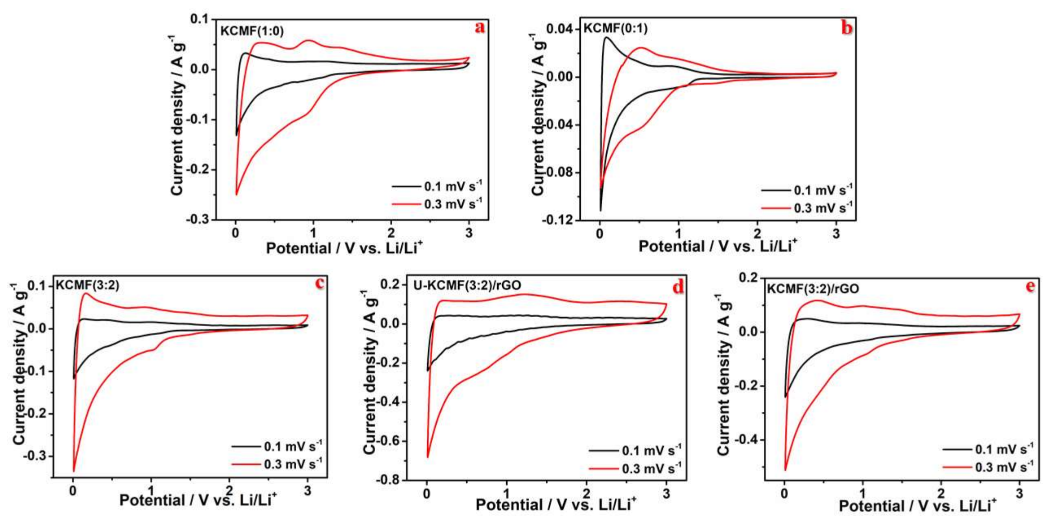

Figure S19. The comparison of CV plots for the 3rd cycle at 0.1 and 0.3 mV s^{-1} of KCMF(1:0) (a), (0:1) (b), (3:2) (c) U-KCMF(3:2)/rGO (d) and KCMF(3:2)/rGO (e) electrodes.

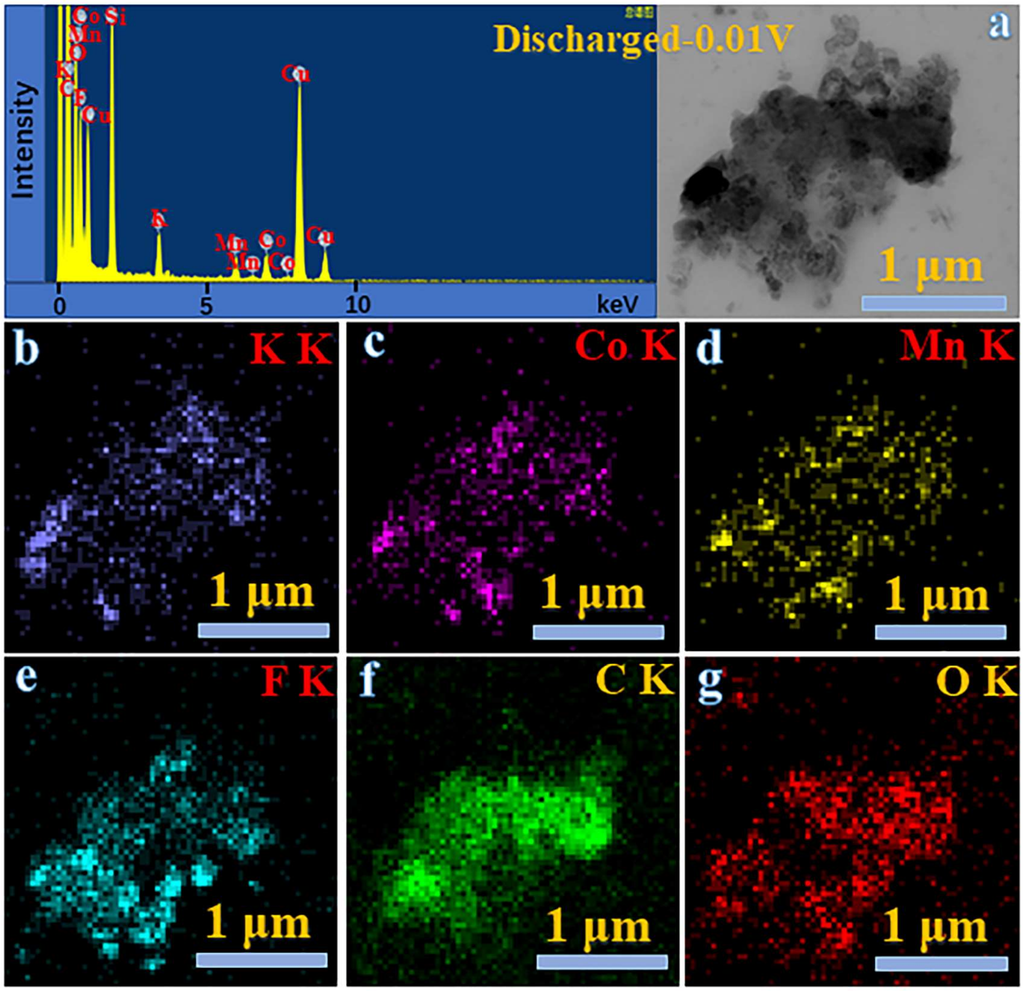

Figure S20. EDS (a), and mapping (b-g) for the KCMF(3:2) electrode discharged-0.01V state of the first GCD (0.05 A g^{-1}) cycle.

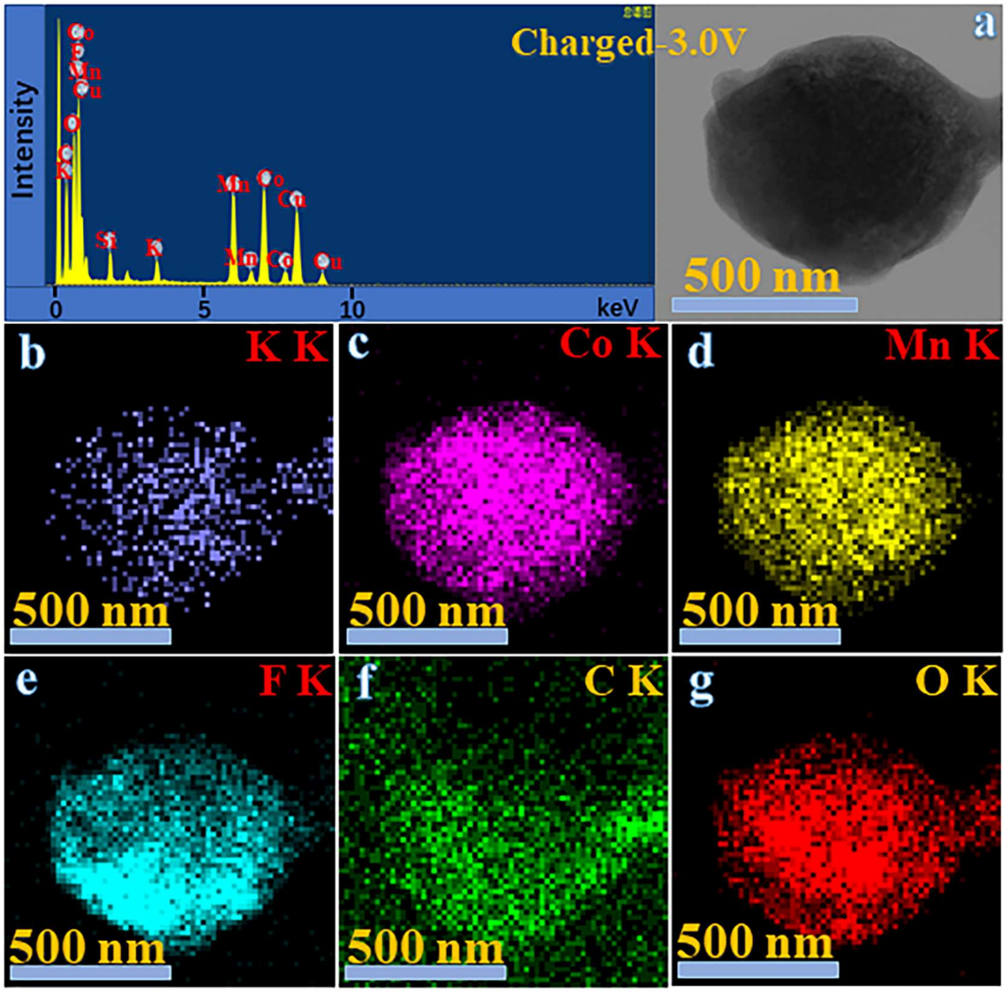

Figure S21. EDS (a), and mapping (b-g) for the KCMF(3:2) electrode charged-3.0V state of the first GCD (0.05 A g^{-1}) cycle.

(a)

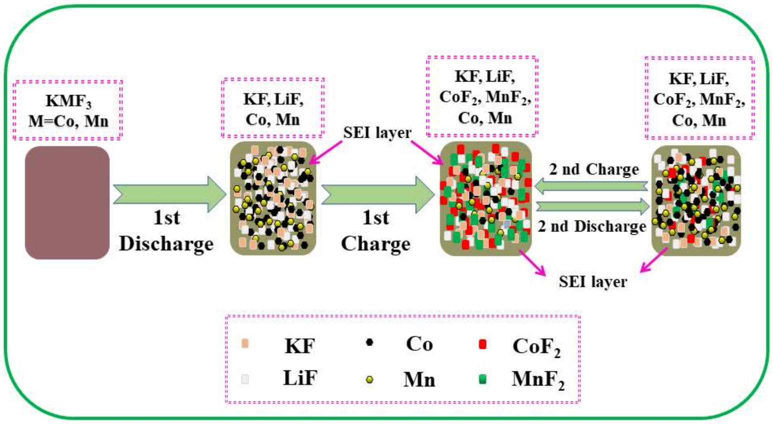

(b)

Phases	PDF Card	Crystal system	Space group	Cell (a×b×c)/Å^3
Co	05-0727	Hexagonal	P63/mmc	2.503×2.503×4.061
Mn	17-0910	Tetragonal	I4/mmm	2.672×2.672×3.550
CoF_2	38-0883	Cubic	Pa-3	4.958×4.958×4.958
MnF_2	34-1326	Tetragonal	P-42m	5.112×5.112×5.256
LiF	45-1460	Cubic	Fm-3m	4.027×4.027×4.027
KF	36-1458	Cubic	Fm-3m	5.348×5.348×5.348
Li_2CO_3	22-1141	Monoclinic	C2/c (15)	8.359×4.977×6.194

Figure S22. Schematics of reaction mechanisms for KCMF(3:2) electrode during the discharging/charging processes under the first two cycles (a); Crystalline structure information of Co, Mn, CoF_2, MnF_2, LiF, KF and Li_2CO_3 phases (b).

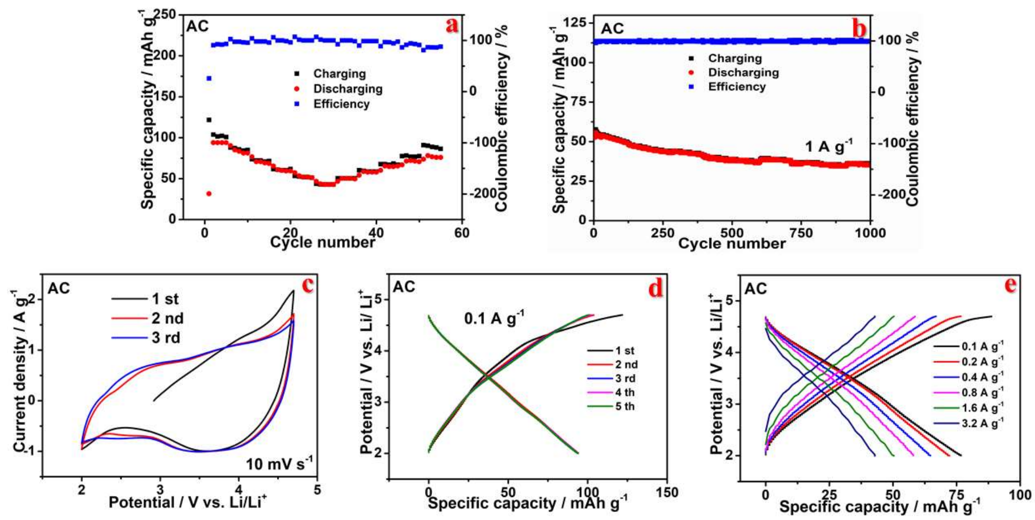

Figure S23. Rate performance and coulombic efficiency at 0.1~3.2~0.1 A g^{-1} (a), cycling stability and coulombic efficiency at 1 A g^{-1} for 1000 cycles (b), CV plots for the first three cycles at 10 mV s^{-1} (c), GCD curves for the first five cycles at 0.1 A g^{-1} (d) and GCD curves for the respective 3rd cycles at 3.2~0.1 A g^{-1} (e) of AC electrode.

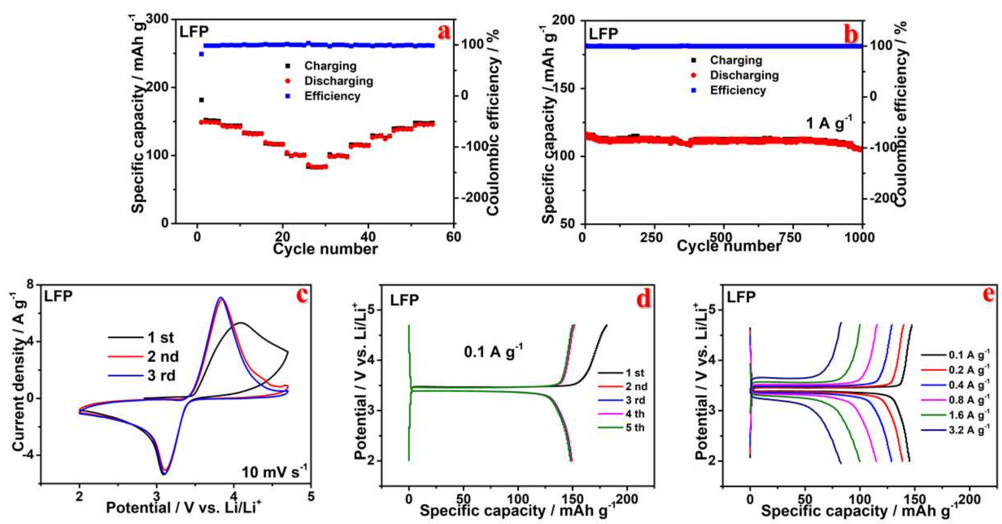

Figure S24. Rate performance and coulombic efficiency at 0.1~3.2~0.1 A g^{-1} (a), cycling stability and coulombic efficiency at 1 A g^{-1} for 1000 cycles (b), CV plots for the first three cycles at 10 mV s^{-1} (c), GCD curves for the first five cycles at 0.1 A g^{-1} (d) and GCD curves for the respective 3rd cycles at 3.2~0.1 A g^{-1} (e) of LFP electrode.

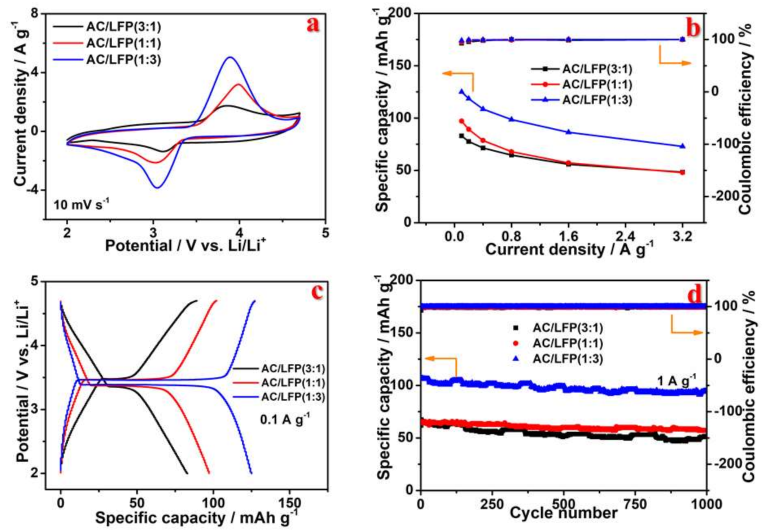

Figure S25. The comparisons of CV plots at 10 mV s^{-1} (a), specific capacity and coulombic efficiency derived from the respective 3rd cycle at 3.2-0.1 A g^{-1} (b), GCD curves for the 3rd cycle at 0.1 A g^{-1} (c) and cycling stability for 1000 cycles at 1 A g^{-1} (d) between AC/LFP(3:1), (1:1) and (1:3) electrodes.

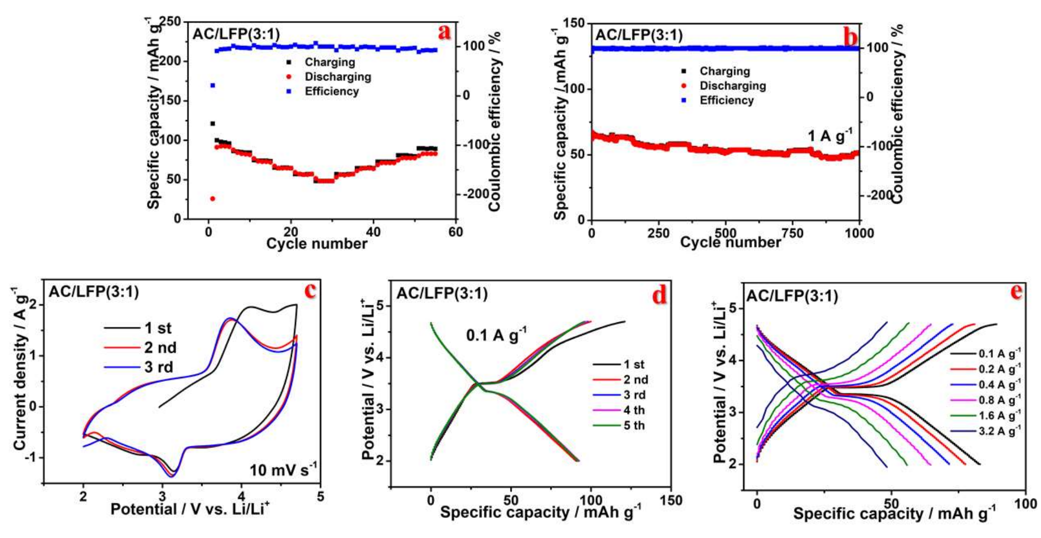

Figure S26. Rate performance and coulombic efficiency at 0.1~3.2~0.1 A g^{-1} (a), cycling stability and coulombic efficiency at 1 A g^{-1} for 1000 cycles (b), CV plots for the first three cycles at 10 mV s^{-1} (c), GCD curves for the first five cycles at 0.1 A g^{-1} (d) and GCD curves for the respective 3rd cycles at 3.2~0.1 A g^{-1} (e) of AC/LFP(3:1) electrode.

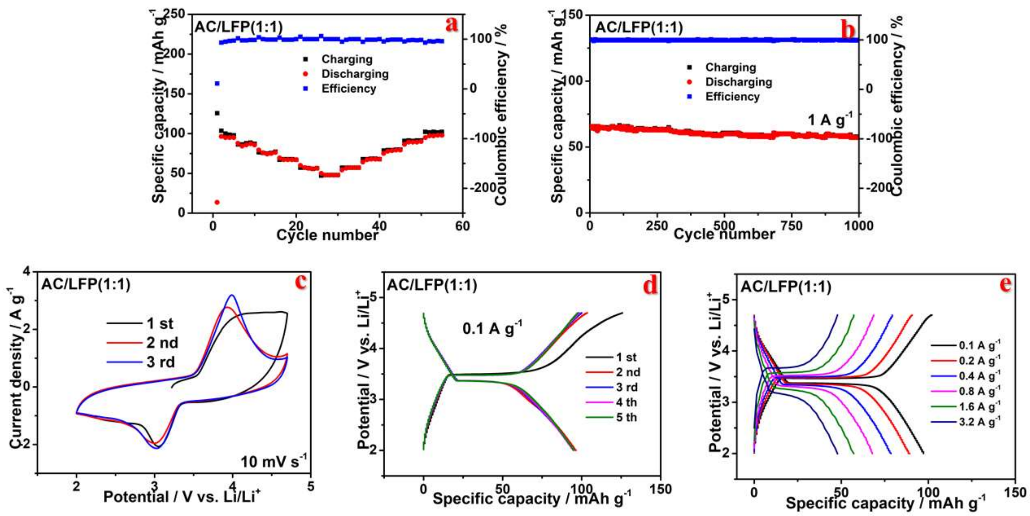

Figure S27. Rate performance and coulombic efficiency at 0.1~3.2~0.1 A g^{-1} (a), cycling stability and coulombic efficiency at 1 A g^{-1} for 1000 cycles (b), CV plots for the first three cycles at 10 mV s^{-1} (c), GCD curves for the first five cycles at 0.1 A g^{-1} (d) and GCD curves for the respective 3rd cycles at 3.2~0.1 A g^{-1} (e) of AC/LFP(1:1) electrode.

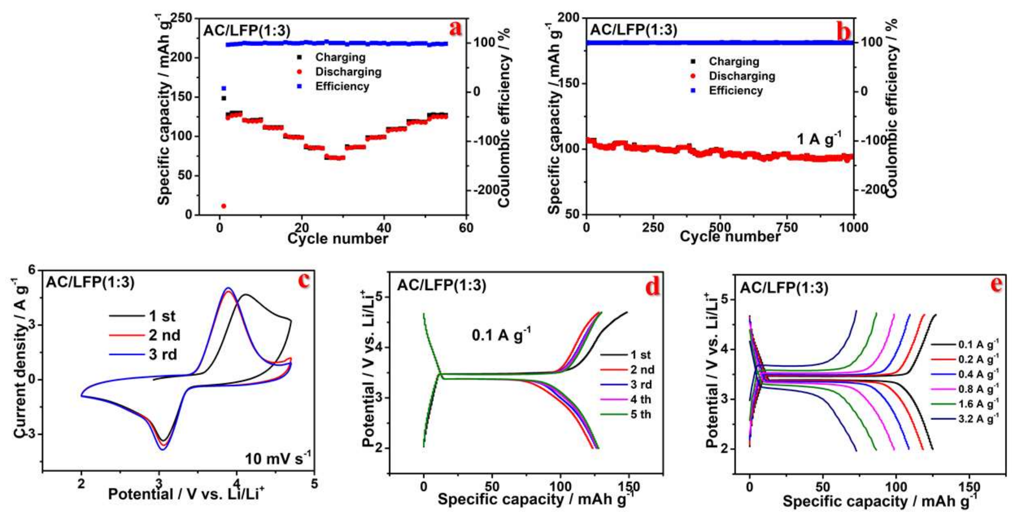

Figure S28. Rate performance and coulombic efficiency at 0.1~3.2~0.1 A g^{-1} (a), cycling stability and coulombic efficiency at 1 A g^{-1} for 1000 cycles (b), CV plots for the first three cycles at 10 mV s^{-1} (c), GCD curves for the first five cycles at 0.1 A g^{-1} (d) and GCD curves for the respective 3rd cycles at 3.2~0.1 A g^{-1} (e) of AC/LFP(1:3) electrode.

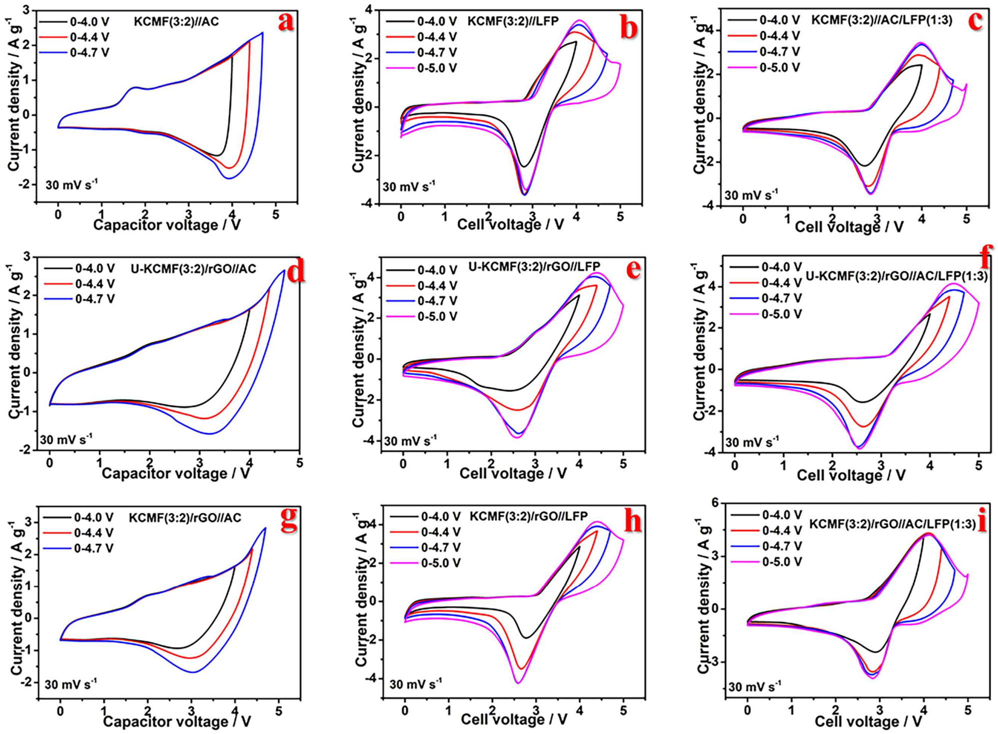

Figure S29. CV windows at 30 mV s^{-1} of KCMF(3:2)//AC, U-KCMF(3:2)/rGO//AC and KCMF(3:2)/rGO//AC LICs (a, d, g); KCMF(3:2)//LFP, U-KCMF(3:2)/rGO//LFP and KCMF(3:2)/rGO//LFP LIBs (b, e, h); KCMF(3:2)//AC/LFP(1:3), U-KCMF(3:2)/rGO//AC/LFP(1:3) and KCMF(3:2)/rGO//AC/LFP(1:3) LIC/Bs (c, f, i).

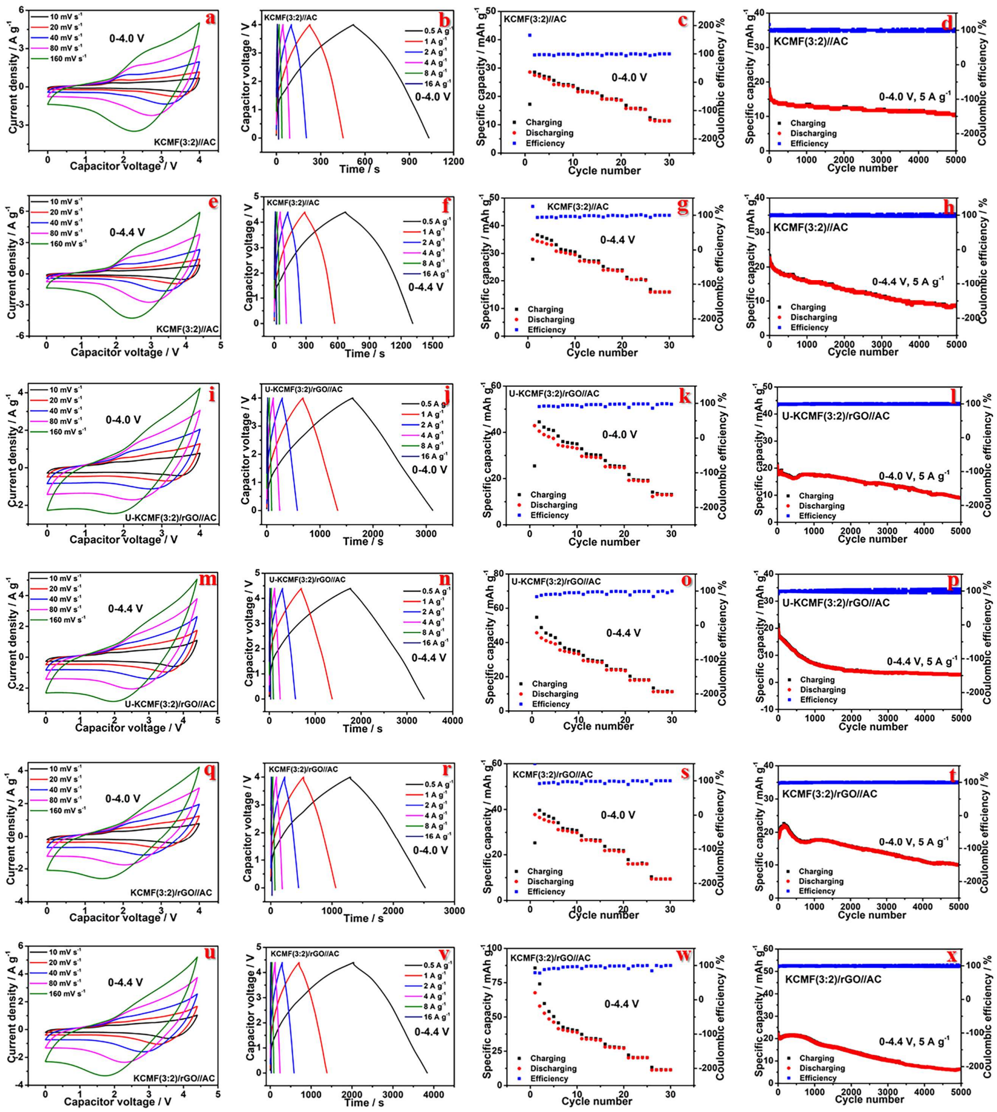

Figure S30. CV plots at 10~160 mV s^{-1}, GCD curves at 0.5~16 A g^{-1}, rate performance and coulombic efficiency at 0.5~16 A g^{-1} and cycling stability and coulombic efficiency at 5 A g^{-1} for 5000 cycles of KCMF(3:2)//AC LICs under the working voltages of 0~4.0 V (a-d), 0~4.4 V (e-h), U-KCMF(3:2)/rGO//AC LICs under the working voltages of 0~4.0 V (i-l), 0~4.4 V (m-p) and KCMF(3:2)/rGO//AC LICs under the working voltages of 0~4.0 V (q-t), 0~4.4 V (u-x).

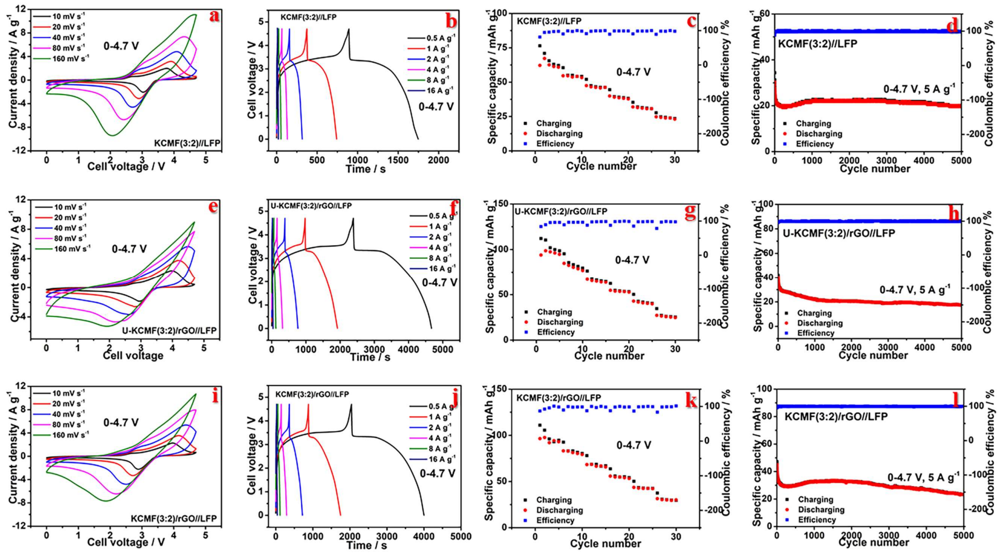

Figure S31. CV plots at 10~160 mV s^{-1}, GCD curves at 0.5~16 A g^{-1}, rate performance and coulombic efficiency at 0.5~16 A g^{-1} and cycling stability and coulombic efficiency at 5 A g^{-1} for 5000 cycles under the working voltage of 0~4.7 V of KCMF(3:2)//LFP LIBs (a-d), U-KCMF(3:2)/rGO//LFP LIBs (e-h) and KCMF(3:2)/rGO//LFP LIBs (i-l).

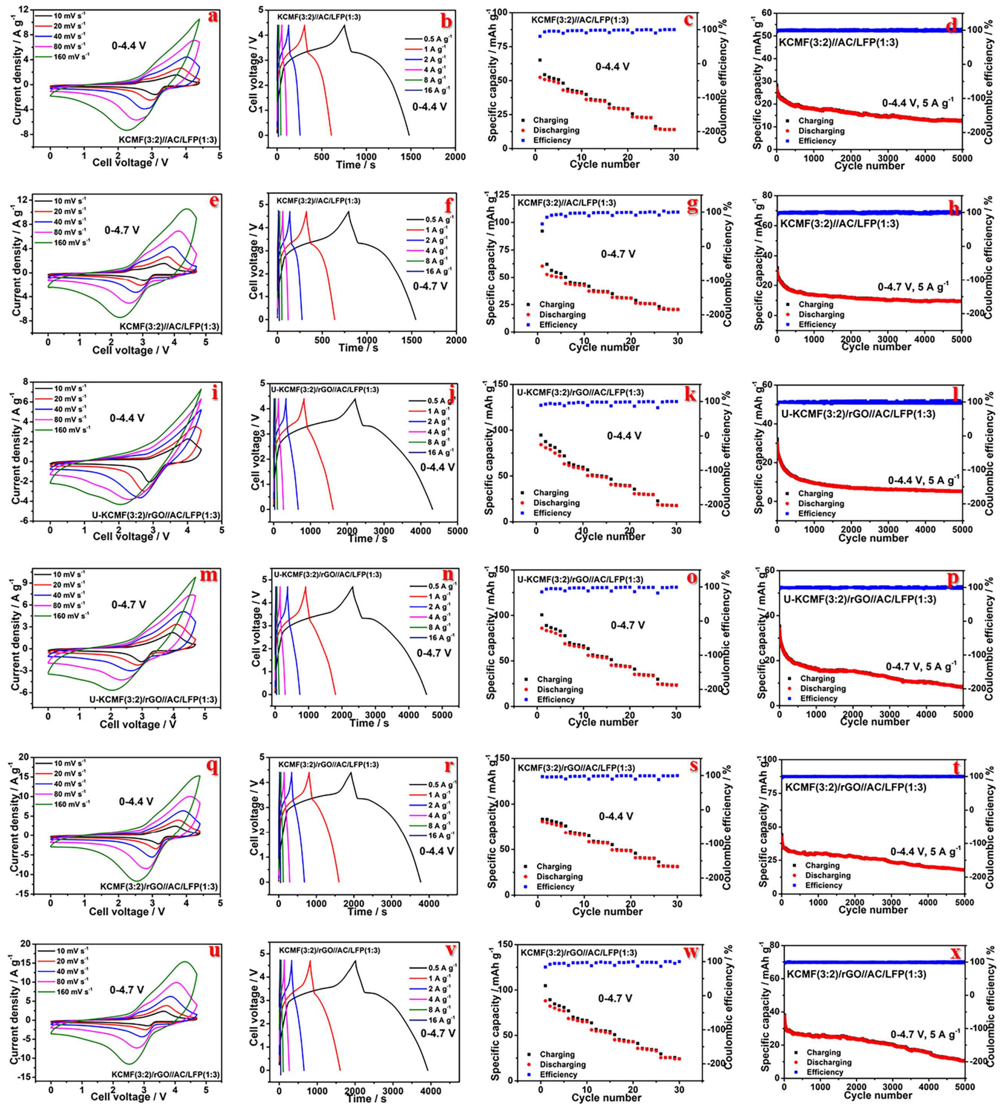

Figure S32. CV plots at 10~160 mV s^{-1}, GCD curves at 0.5~16 A g^{-1}, rate performance and coulombic efficiency at 0.5~16 A g^{-1} and cycling stability and coulombic efficiency at 5 A g^{-1} for 5000 cycles of KCMF(3:2)//AC/LFP(1:3) LIC/Bs under the working voltages of 0~4.4 V (a-d), 0~4.7 V (e-h), U-KCMF(3:2)/rGO//AC/LFP(1:3) LIC/Bs under the working voltages of 0~4.4 V (i-l), 0~4.7 V (m-p) and KCMF(3:2)/rGO//AC/LFP(1:3) LIC/Bs under the working voltages of 0~4.4 V (q-t), 0~4.7 V (u-x).

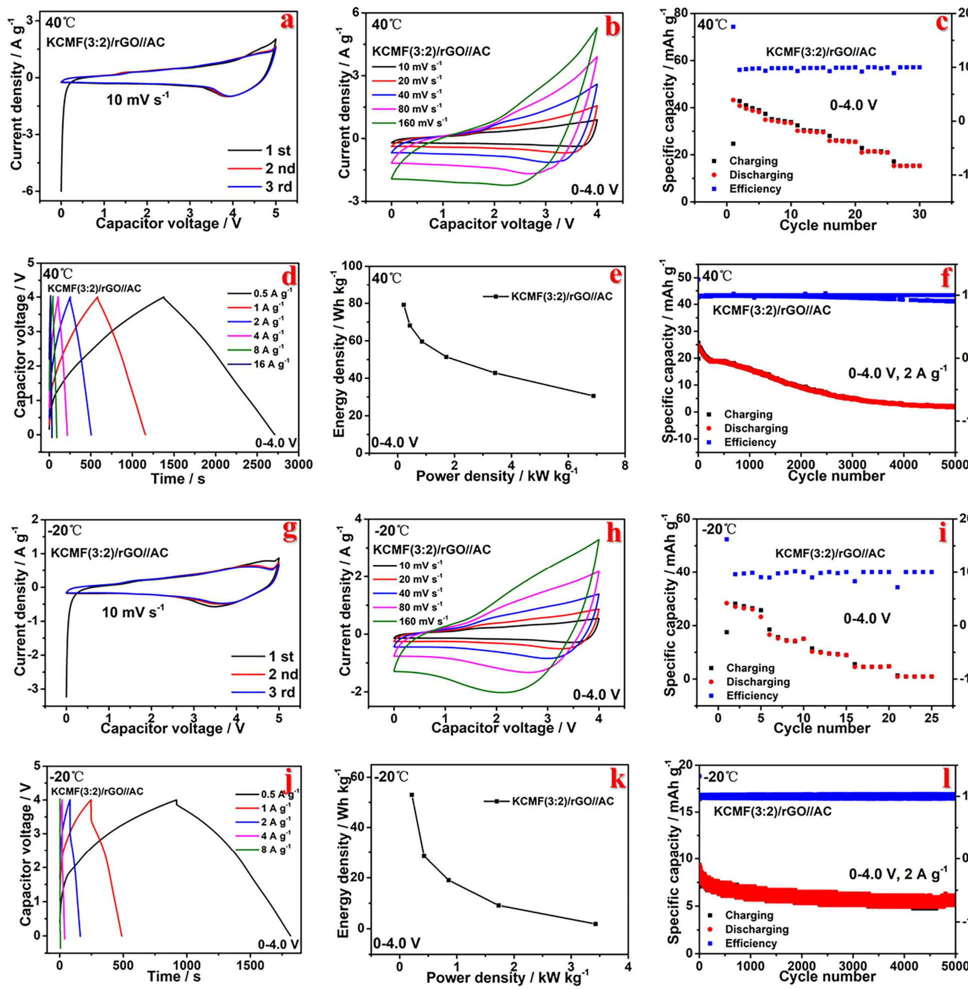

Figure S33. The performance of KCMF(3:2)/rGO//AC LICs under high (40 ℃) and low (-20 ℃) temperature: CV windows at 10 mV s^{-1} (a, g), CV plots at 10-160 mV s^{-1} (b, h), rate performance (c, i), GCD curves (d, j), Ragone plots (e, k) and cycling behavior at 2 A g^{-1} for 5000 cycles (f, l) under the working voltage of 0-4.0 V.

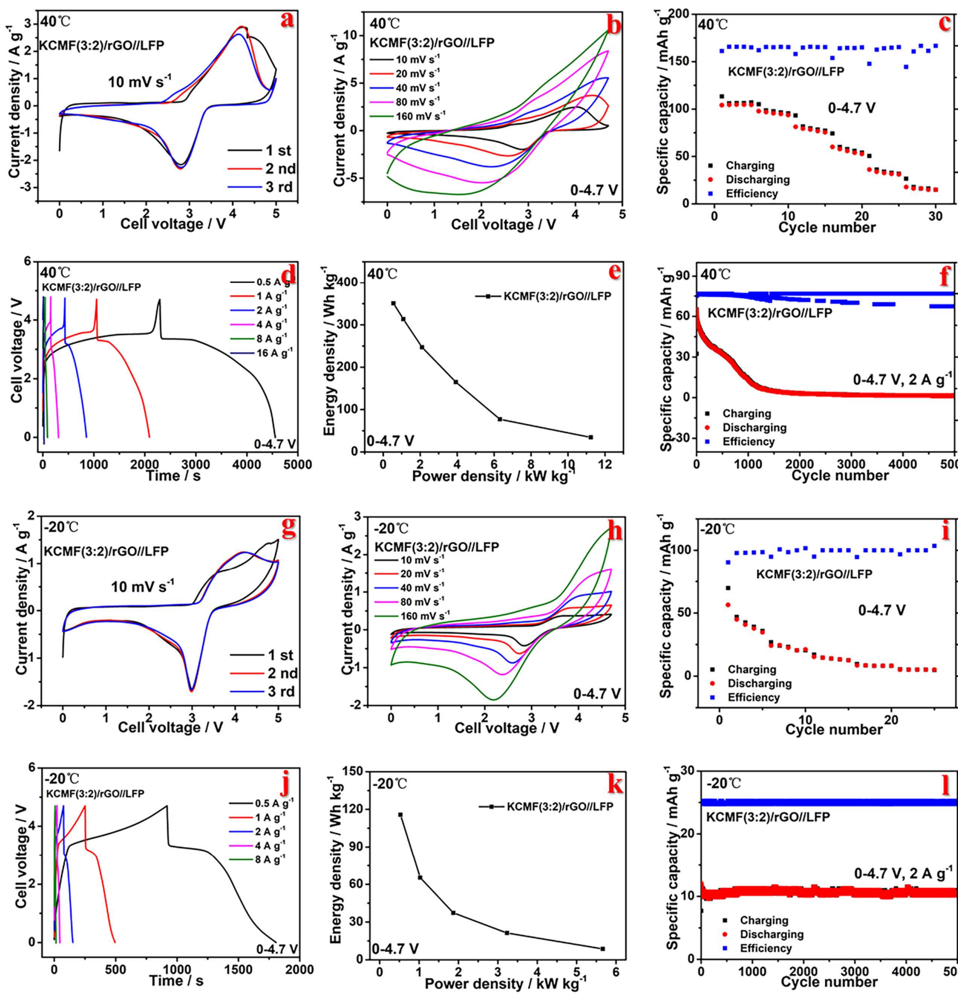

Figure S34. The performance of KCMF(3:2)/rGO//LFP LIBs under high (40℃) and low (-20℃) temperature: CV windows at 10 mV s^{-1} (a, g), CV plots at 10-160 mV s^{-1} (b, h), rate performance (c, i), GCD curves (d, j), Ragone plots (e, k) and cycling behavior at 2 A g^{-1} for 5000 cycles (f, l) under the working voltage of 0-4.7 V.

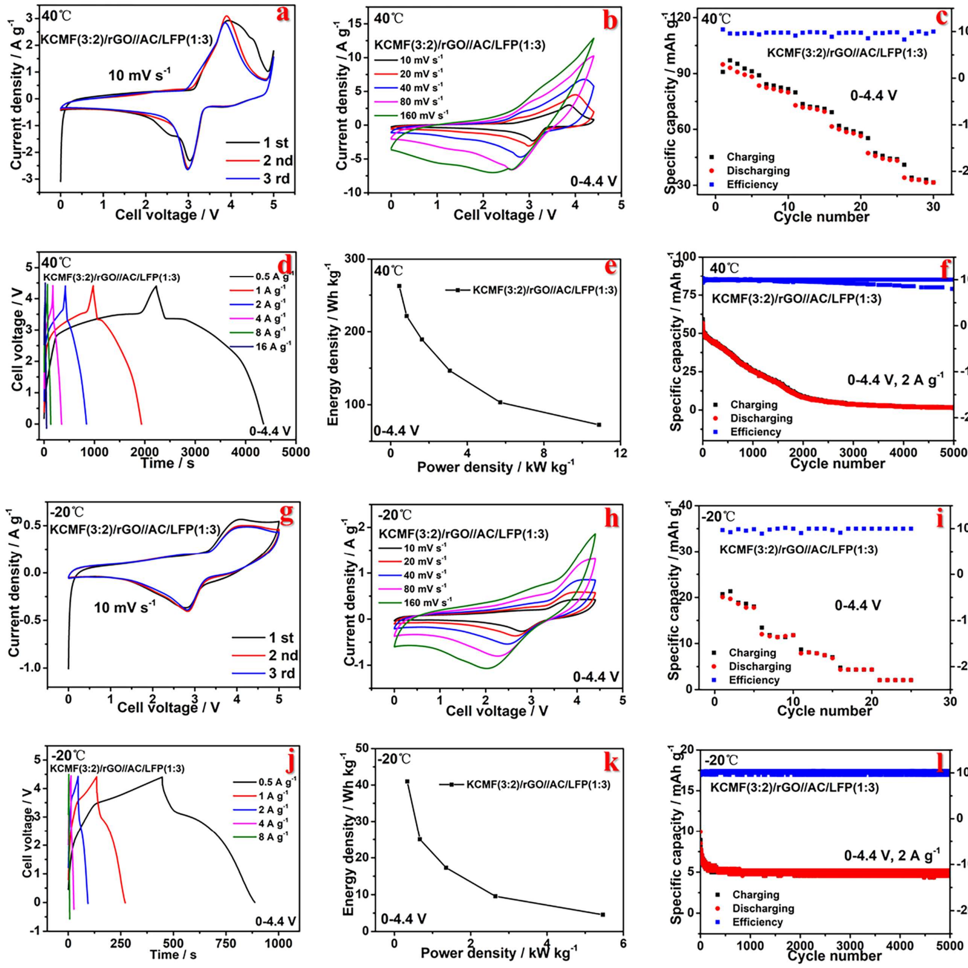

Figure S35. The performance of KCMF(3:2)/rGO//AC/LFP(1:3) LIC/Bs under high (40℃) and low (-20℃) temperature: CV windows at 10 mV s^{-1} (a, g), CV plots at 10-160 mV s^{-1} (b, h), rate performance (c, i), GCD curves (d, j), Ragone plots (e, k) and cycling behavior at 2 A g^{-1} for 5000 cycles (f, l) under the working voltage of 0-4.4 V.

Supplemental tables

Table S1. Materials, chemicals and reagents used in this study.

Materials, chemicals and reagents	Type	Company	Characteristics
$CoCl_2\cdot 6H_2O$	AR	SinoPharm	Purity≥99.0%
$MnCl_2\cdot 4H_2O$	AR	SinoPharm	Purity≥99.0%
$KF\cdot 2H_2O$	AR	SinoPharm	Purity≥99.0%
PVP-K30	GR	SinoPharm	Purity≥99.8%
EG	AR	SinoPharm	Purity≥99.0%
Graphene oxide (GO)	Powder	ZhengZhou JingHong New Energy	Purity≥94.0% 3-10 floors Conductivity: $2.0*10^5$ S m^{-1} SSA: 150~200 m^2 g^{-1}
AC	YEC 8b	FuZhou YiHuan	D50: ~10 μm; Density: 0.4 g cm^{-3}; SSA: 2000~2500 m^2 g^{-1}
$LiFePO_4$	LFP-NCO	Aleees	D50: 4 ± 2 μm; Tab: 1 ± 0.2 g cm^{-3}; SSA: 13 ± 2 m^2 g^{-1}
AB	Battery grade	#	#
NMP	AR	Kermel	Purity≥99.0%
PVDF	Battery grade	#	#
Electrolytes	LBC-305-01	CAPCHEM	1 M $LiPF_6$/EC: EMC: DMC (1:1:1)/1% VC
Li plate	15.6*0.45 mm	China Energy	15.6*0.45 mm
Cu foil	200*0.015	GuangZhou JiaYuan	Total thickness: 15 μm; Weight: 87 g m^{-2}
Carbon coated-Al foil	222*0.015	GuagZhou NaNuo	Total thickness: 17 μm; Strength: 192 Mpa
Glass microfiber filters	GF/D 2.7 μm 1823-025	Whatman	Diameter: 25 mm; Thickness: 675 μm; Weight: 121 g m^{-2}
Cell components	CR-2032	ShenZhen TianChenHe	#

Table S2. ICP results of KCMF(3:2) (a), U-KCMF(3:2)/rGO (b) and KCMF(3:2)/rGO (c) samples.

(a)

Sample	Element	Wt.%	The final chemical composition
KCMF(3:2)	K	24.99	$K_{0.97}Co_{0.55}Mn_{0.45}F_{2.96}$
	Co	21.40	
	Mn	16.41	
	F	37.20	

(b)

Sample	Element	Wt.%	The final chemical composition
U-KCMF(3:2)/rGO	K	18.70	$K_{0.93}Co_{0.54}Mn_{0.46}F_{3.0}$
	Co	16.84	
	Mn	12.89	

(c)

Sample	Element	Wt.%	The final chemical composition
KCMF(3:2)/rGO	K	18.20	$K_{1.02}Co_{0.54}Mn_{0.46}F_{3.0}$
	Co	14.45	
	Mn	11.52	

Table S3. Specific capacity of KCMF (Co/Mn=1:0~0:1), U-KCMF(3:2)/rGO and KCMF(3:2)/rGO electrodes.

***i*/(A g^{-1})**	**Specific capacity/(mAh g^{-1})**										
	KCMF electrodes (Co/Mn=1:0~0:1)									**U-(3:2)/rGO**	**(3:2)/rGO**
	1:0	**6:1**	**3:1**	**3:2**	**1:1**	**2:3**	**1:3**	**1:6**	**0:1**		
0.1	144	109	108	**126**	108	101	88	88	76	**339**	**288**
0.2	123	91	89	**106**	92	87	79	77	71	**288**	**259**
0.4	98	72	75	**87**	77	75	71	68	64	**230**	**215**
0.8	71	58	62	**71**	64	63	61	60	55	**180**	**177**
1.6	51	44	48	**56**	51	52	51	48	45	**134**	**138**
3.2	36	32	36	**41**	39	40	40	38	36	**92**	**106**
Cycling behavior retention%/2 A g^{-1}/ 1000 cycles	190	207	213	**232**	175	188	187	182	183	**125**	**169**

Table S4. A comparison for reported perovskite fluorides anodes for lithium-ion storage.

i/(A g^{-1})	Specific capacity (mAh g^{-1})		
	$KCo_{0.54}Mn_{0.46}F_3$/rGO This work	**$KNi_{0.1}Co_{0.9}F_3$** [1]. *J. Mater. Chem. A*, 2019, **7**, 8315-8326	**$Na_{0.85}Ni_{0.45}Co_{0.55}F_{3.56}$** [2]. *Chem. Commun.*, 2019, **55**, 6739-6742
0.1	**288**	166	286
0.2	**259**	161	250
0.4	**215**	147	219
0.8	**177**	124	184
1.6	**138**	99	149
3.2	**106**	73	115
Cycling behavior retention	**169%/1000 cycles/ 2 A g^{-1}**	197%/1000 cycles/1 A g^{-1}	187%/600 cycles/1 A g^{-1}

Table S5. EIS parameters of KCMF(3:2), U-KCMF(3:2)/rGO and KCMF(3:2)/rGO electrodes before (a) and after (b) cycling.

(a)

EIS parameters			
Before cycling	**KCMF(3:2)**	**U-KCMF(3:2)/rGO**	**KCMF(3:2)/rGO**
Model		$R(QR)W(QR)$	
R_s (Ω)	3.346	5.074	3.173
Q_1 (S·sec^n)	1.556×10^{-5}	2.045×10^{-5}	2.7×10^{-5}
n_1	0.8554	0.8288	0.8069
R_{ct} (Ω)	63.75	49.63	47.21
W (S·sec$^{0.5}$)	0.01631	0.009539	0.008319
Q_2 (S·sec^n)	5.951×10^{-4}	9.446×10^{-4}	1.183×10^{-3}
n_2	0.9738	0.9715	0.9629
R_e (Ω)	6.984×10^{5}	3.305×10^{5}	3.127×10^{5}
χ^2	3.049×10^{-3}	2.461×10^{-3}	2.82×10^{-3}

(b)

EIS parameters			
After cycling	**KCMF(3:2)**	**U-KCMF(3:2)/rGO**	**KCMF(3:2)/rGO**
Model		$R(CR)(CR)(Q(RW))C$	
R_s (Ω)	4.451	6.549	7.972
$C_{dl,1}$ (F)	5.965×10^{-6}	2.494×10^{-5}	1.257×10^{-5}
R_{SEI} (Ω)	2.66	3.507	4.429
$C_{dl,2}$ (F)	7.51×10^{-3}	2.983×10^{-6}	4.747×10^{-3}
$R_{ct,1}$ (Ω)	6.086	4.934	8.754
Q (S·sec^n)	1.564×10^{-4}	2.242×10^{-3}	1.05×10^{-4}
n	0.7445	0.5587	0.7648
$R_{ct,2}$ (Ω)	36.21	29.66	49.36
W (S·sec$^{0.5}$)	0.02694	0.04528	0.01931
C_{int} (F)	0.01972	0.08658	0.02547
χ^2	7.584×10^{-4}	3.183×10^{-4}	3.914×10^{-4}

Table S6. Specific capacity of positive electrodes (AC, LFP, AC/LFP(3:1), AC/LFP(1:1) and AC/LFP(1:3)).

***i*/(A g^{-1})**	**Specific capacity/(mAh g^{-1})**				
	AC	**LFP**	**AC/LFP(3:1)**	**AC/LFP(1:1)**	**AC/LFP(1:3)**
0.1	**77**	**145**	83	97	**125**
0.2	**72**	**139**	78	89	**119**
0.4	**65**	**129**	71	79	**109**
0.8	**58**	**115**	65	68	**99**
1.6	**50**	**100**	56	57	**86**
3.2	**43**	**83**	48	48	**73**
Cycling behavior retention%/1 A g^{-1}/ 1000 cycles	**71**	**92**	78	89	**89**

Table S7. Design of m_+/m_- ratios for KCMF(3:2)//AC, U-KCMF(3:2)/rGO//AC, KCMF(3:2)/rGO//AC LICs, KCMF(3:2)//LFP, U-KCMF(3:2)/rGO//LFP, KCMF(3:2)/rGO//LFP LIBs and KCMF(3:2)//AC/LFP(1:3), U-KCMF(3:2)/rGO//AC/LFP(1:3), KCMF(3:2)/rGO//AC/LFP(1:3) LIC/Bs.

Energy storage devices	Name	Q_m(mAh g^{-1}, 0.1A/g)						m_+/m_-
		Positive electrode			Negative electrode			
		AC	LFP	AC/LFP (1:3)	KCMF (3:2)	U-KCMF (3:2)/rGO	KCMF (3:2)/rGO	
Lithium-ion capacitors (LICs)	KCMF(3:2) //AC	77			126			**1.6:1**
	U-KCMF(3:2)/rGO //AC	77				339		**4.4:1**
	KCMF(3:2)/rGO //AC	77					288	**3.7:1**
Lithium-ion batteries (LIBs)	KCMF(3:2) //LFP		145		126			**0.9:1**
	U-KCMF(3:2)/rGO //LFP		145			339		**2.3:1**
	KCMG (3:2)/rGO //LFP		145				288	**2.0:1**
Lithium-ion capacitor/battery hybrids (LIC/Bs)	KCMF(3:2) //AC/LFP(1:3)			125	126			**1:1**
	U-KCMF(3:2)/rGO //AC/LFP(1:3)			125		339		**2.7:1**
	KCMF(3:2)/rGO //AC/LFP(1:3)			125			288	**2.3:1**

Table S8. Performance summary of different energy storage devices in this study: KCMF(3:2)//AC, U-KCMF(3:2)/rGO//AC, KCMF(3:2)/rGO//AC LICs (a), KCMF(3:2)//LFP, U-KCMF(3:2)/rGO//LFP, KCMF(3:2)/rGO//LFP LIBs (b) and KCMF(3:2)//AC/LFP(1:3), U-KCMF(3:2)/rGO//AC/LFP(1:3), KCMF(3:2)/rGO//AC/LFP(1:3) LIC/Bs (c).

(a)

LICs	Working voltage/V	Energy density/ Wh kg^{-1}	Power density/ kW kg^{-1}	Cycling behavior/ retention%, repeated cycles, current density
KCMF(3:2)//AC	0~4.0	54.2~47.6 43.2~38.1 31.5~22.7	0.4~0.8 1.6~3.1 6.2~12.2	74%/1000/5A g^{-1} 70%/2000/5A g^{-1} 66%/3000/5A g^{-1} 60%/5000/5A g^{-1}
	0~4.4	75.0~66.4 59.3~52.9 45.0~35.0	0.4~0.9 1.7~3.4 6.8~13.7	70%/1000/5A g^{-1} 59%/2000/5A g^{-1} 49%/3000/5A g^{-1} 37%/5000/5A g^{-1}
U-KCMF(3:2)/rGO //AC	0~4.0	78.0~67.6 58.6~49.7 38.1~25.9	0.2~0.4 0.8~1.5 3.0~6.0	83%/1000/5A g^{-1} 75%/2000/5A g^{-1} 67%/3000/5A g^{-1} 43%/5000/5A g^{-1}
	0~4.4	90.4~75.7 63.6~52.8 39.6~24.8	0.2~0.4 0.8~1.6 3.3~6.5	34%/1000/5A g^{-1} 23%/2000/5A g^{-1} 18%/3000/5A g^{-1} 14%/5000/5A g^{-1}
KCMF(3:2)/rGO //AC	0~4.0	71.1~61.3 52.6~43.6 32.0~18.8	0.2~0.4 0.8~1.7 3.4~6.8	94%/1000/5A g^{-1} 84%/2000/5A g^{-1} 72%/3000/5A g^{-1} 53%/5000/5A g^{-1}
	0~4.4	115.9~87.7 74.4~60.8 44.7~24.8	0.2~0.5 0.9~1.9 3.7~7.4	83%/1000/5A g^{-1} 65%/2000/5A g^{-1} 47%/3000/5A g^{-1} 29%/5000/5A g^{-1}

(b)

LIBs	Working voltage/V	Energy density/ Wh kg^{-1}	Power density/ kW kg^{-1}	Cycling behavior/ retention%, repeated cycles, current density
KCMF(3:2)//LFP	0~4.7	209.7~177.5 151.1~123.7 96.7~69.0	0.9~1.7 3.5~6.8 13.2~24.3	72%/1000/5A g^{-1} 72%/2000/5A g^{-1} 72%/3000/5A g^{-1} 65%/5000/5A g^{-1}
U-KCMF(3:2)/rGO //LFP	0~4.7	325.7~263.2 202.3~154.3 102.3~51.6	0.5~1.0 1.9~3.6 6.2~9.9	56%/1000/5A g^{-1} 51%/2000/5A g^{-1} 47%/3000/5A g^{-1} 43%/5000/5A g^{-1}
KCMF(3:2)/rGO //LFP	0~4.7	307.6~266.1 210.4~158.0 112.5~68.6	0.6~1.1 2.1~3.9 7.2~12.4	72%/1000/5A g^{-1} 72%/2000/5A g^{-1} 64%/3000/5A g^{-1} 52%/5000/5A g^{-1}

(c)

LIC/Bs	Working voltage/V	Energy density/ Wh kg^{-1}	Power density/ kW kg^{-1}	Cycling behavior/ retention%, repeated cycles, current density
KCMF(3:2) //AC/LFP(1:3)	0~4.4	147.6~121.0 100.5~78.5 57.0~28.0	0.7~1.5 2.9~5.4 10.0~16.0	66%/1000/5A g^{-1} 60%/2000/5A g^{-1} 53%/3000/5A g^{-1} 46%/5000/5A g^{-1}
	0~4.7	150.0~123.9 103.6~86.4 69.8~51.1	0.7~1.4 2.8~5.6 10.9~20.0	45%/1000/5A g^{-1} 40%/2000/5A g^{-1} 33%/3000/5A g^{-1} 31%/5000/5A g^{-1}
U-KCMF(3:2)/rGO //AC/LFP(1:3)	0~4.4	218.6~157.2 124.1~95.1 69.4~36.3	0.4~0.7 1.4~2.6 5.0~8.7	31%/1000/5A g^{-1} 23%/2000/5A g^{-1} 20%/3000/5A g^{-1} 17%/5000/5A g^{-1}
	0~4.7	243.6~183.0 135.9~106.4 79.1~49.7	0.4~0.7 1.3~2.6 5.0~9.0	48%/1000/5A g^{-1} 45%/2000/5A g^{-1} 36%/3000/5A g^{-1} 24%/5000/5A g^{-1}
KCMF(3:2)/rGO //AC/LFP(1:3)	0~4.4	229.1~187.8 159.0~131.1 104.7~78.7	0.4~0.9 1.7~3.3 6.3~12.2	71%/1000/5A g^{-1} 65%/2000/5A g^{-1} 56%/3000/5A g^{-1} 42%/5000/5A g^{-1}
	0~4.7	234.7~190.1 149.5~113.6 85.4~57.5	0.4~0.9 1.7~3.2 6.0~10.9	68%/1000/5A g^{-1} 62%/2000/5A g^{-1} 54%/3000/5A g^{-1} 28%/5000/5A g^{-1}

Table S9. A comparison for some reported LICs (a) and LIBs (b).

(a)

LICs	Working voltage/V	Energy density/ Wh kg^{-1}	Power density/ kW kg^{-1}	Cycling behavior/ retention%, repeated cycles, current density	Refs
Li_3VO_4/N-C//AC	1.0-4.0	136.4-24.4	0.532-11.02	87%/1500/2 A g^{-1}	[3]. *Adv. Mater.*, 2017, **29**, 1700142
$TiNb_2O_7$@C//CFs	0.8-3.2	110.4-20	0.1-5.46	77%/1500/0.2 A g^{-1}	[4]. *Nano Energy*, 2015, **15**, 104-115
TiO_2 belt//Graphene	0-3.8	82-21	0.57-19	73%/600/1 A g^{-1}	[5]. *Small*, 2015, **11**, 1470-1477
$LiNi_{0.5}Mn_{1.5}O_4$//AC	1.5-3.25	19-8	0.13-3.5	81%/3000/1 A g^{-1}	[6]. *Nano Energy*, 2015, **12**, 69-75
TiO_2@EEG//EEG	0.0-3.0	72-10	0.303-2.0	68%/1000/1.5 A g^{-1}	[7]. *Small*, 2016, **12**, 6207-6213
KCMF(3:2)/rGO //AC	**0~4.0**	**71.1~18.8**	**0.2~6.8**	**94%/1000/5A g^{-1} *** **84%/2000/5A g^{-1} ***	**This work**
	0~4.4	**115.9~24.8**	**0.2~7.4**	**83%/1000/5A g^{-1} *** **65%/2000/5A g^{-1} ***	
KCMF(3:2)/rGO //AC/LFP(1:3)	**0~4.4**	**229.1~78.7**	**0.4~12.2**	**71%/1000/5A g^{-1} *** **65%/2000/5A g^{-1} *** **88%/1000/5A g^{-1} #** **81%/2000/5A g^{-1} #**	
	0~4.7	**234.7~57.5**	**0.4~10.9**	**68%/1000/5A g^{-1} *** **62%/2000/5A g^{-1} *** **88%/1000/5A g^{-1} #** **81%/2000/5A g^{-1} #**	

Note: * Based on the 1st cycle;
 # Based on the 50th cycle.

(b)

LIBs	Working voltage/V	Energy density/ Wh kg^{-1}	Power density/ kW kg^{-1}	Cycling behavior/ retention%, repeated cycles, current density	Refs
Si/graphene// $LiNi_{1/3}Co_{1/3}Mn_{1/3}O_2$	3-4.3	156	0.03	70.4%/15/ 0.0375 A g^{-1}	[8]. *Nano Energy*, 2012, **1**, 164-171
$Li_4Ti_5O_{12}$-$Li_2Ti_3O_7$//LFP	1.9-2.5	75	0.048	#	[9]. *Adv. Funct. Mater.*, 2013, **23**, 640-647
Sn-C //Li[$Ni_{0.45}Co_{0.1}Mn_{1.45}O_4$]	3.1-4.8	170	0.18	#	[10]. *J. Am. Chem. Soc.*, 2011, **133**, 3139-3143
FeSb-TiC//LNMO	2.0-5.0	260	0.127	68%/50/ 0.0365 A g^{-1}	[11]. *Chem. Mater.*, 2014, **26**, 5905-5913
TiO_2-MoO_3//$LiCoO_2$	1.0-4.0	285	1.086	#	[12]. *Adv. Funct. Mater.*, 2015, **25**, 3524-3533
KCMF(3:2)/rGO//LFP	**0~4.7**	**307.6~266.1** **210.4~158.0** **112.5~68.6**	**0.6~1.1** **2.1~3.9** **7.2~12.4**	**72%/2000/5A g^{-1} *** **64%/3000/5A g^{-1} *** **102%/2000/5A g^{-1} #** **90%/3000/5A g^{-1} #** **73%/5000/5A g^{-1} #**	**This work**
KCMF(3:2)/rGO //AC/LFP(1:3)	**0~4.4**	**229.1~187.8** **159.0~131.1** **104.7~78.7**	**0.4~0.9** **1.7~3.3** **6.3~12.2**	**71%/1000/5A g^{-1} *** **65%/2000/5A g^{-1} *** **88%/1000/5A g^{-1} #** **81%/2000/5A g^{-1} #** **69%/30005A g^{-1} #**	
	0~4.7	**234.7~190.1** **149.5~113.6** **85.4~57.5**	**0.4~0.9** **1.7~3.2** **6.0~10.9**	**68%/1000/5A g^{-1} *** **62%/2000/5A g^{-1} *** **88%/1000/5A g^{-1} #** **81%/2000/5A g^{-1} #** **69%/3000/5A g^{-1} #**	

Note: * Based on the 1st cycle;
 # Based on the 50th cycle.

Table S10. A comparison for advanced LICs (a), LIC/Bs (b) and LIBs (c) based on the recently reported perovskite fluorides anodes.

(a)

LICs	Working voltage/V	Energy density/ Wh kg^{-1}	Power density/ kW kg^{-1}	Cycling behavior/ retention%, repeated cycles, current density	Refs
KNCF(1:6)//AC	0~4.5	96~11	0.33~10.5	64%/1000/5 A g^{-1}	[1]. *J. Mater. Chem. A*, 2019, **7**, 8315-8326
NNCF(1:1)//AC	0~4.3	96.1~33.4	0.5~17.2	68%/1000/5 A g^{-1}	[2]. *Chem. Commun.*, 2019, **55**, 6739-6742
KCMF(3:2)/rGO//AC	**0~4.4**	**115.9~24.8**	**0.2~7.4**	**83%/1000/5A g^{-1}**	**This work**

(b)

LIC/Bs	Working voltage/V	Energy density/ Wh kg^{-1}	Power density/ kW kg^{-1}	Cycling behavior/ retention%, repeated cycles, current density	Refs
KNCF(1:6) //AC+LFP(1:1)	0~4.3	110~38	0.4~12.7	73%/1000/5 A g^{-1}	[1]. *J. Mater. Chem. A*, 2019, **7**, 8315-8326
NNCF(1:1) //AC+LFP(1:1)	0~4.6	132.3~53.1	0.6~18.4	82%/1000/5 A g^{-1}	[2]. *Chem. Commun.*, 2019, **55**, 6739-6742
KCMF(3:2)/rGO //AC/LFP(1:3)	**0~4.4**	**229.1~78.7**	**0.4~12.2**	**71%/1000/5A g^{-1} (Based on the 1st cycle)** **88%/1000/5A g^{-1} (Based on the 50th cycle)**	**This work**

(c)

LIBs	Working voltage/V	Energy density/ Wh kg^{-1}	Power density/ kW kg^{-1}	Cycling behavior/ retention%, repeated cycles, current density	Refs
KNCF(1:6)//LFP	0-4.7	173-29	0.75-15.3	67%/2000/2 A g^{-1}	[1]. *J. Mater. Chem. A*, 2019, **7**, 8315-8326
NNCF(1:1)//LFP	1~4.7	196.2~35.2	0.8~19.2	63%/2000/3 A g^{-1}	[2]. *Chem. Commun.*, 2019, **55**, 6739-6742
KCMF(3:2)/rGO//LFP	**0~4.7**	**307.6~68.6**	**0.6~12.4**	**72%/2000/5A g^{-1} (Based on the 1st cycle)** **102%/2000/5A g^{-1} (Based on the 50th cycle)**	**This work**

Table S11. Performance summary of different energy storage devices in this study under high (40 ℃) and low (-20 ℃) temperature: KCMF(3:2)/rGO//AC LICs, KCMF(3:2)/rGO//LFP LIBs and KCMF(3:2)/rGO//AC/LFP(1:3) LIC/Bs.

Energy storage devices	T/°C	Working voltage/V	Energy density/ Wh kg^{-1}	Power density/ kW kg^{-1}	Cycling behavior/ retention%, repeated cycles, current density
KCMF(3:2)/rGO //AC	40	0~4.0V	79.2~68.2 59.6~51.4 42.9~30.6	0.2~0.4 0.9~1.7 3.4~6.9	77%/250/2A g^{-1} 75%/500/2A g^{-1} 65%/1000/2A g^{-1}
	-20		53.0~28.6 19.0~9.1~1.9	0.2~0.4 0.9~1.7~3.4	82%/1000/2A g^{-1} 77%/2000/2A g^{-1} 75%/3000/2A g^{-1} 66%/5000/2A g^{-1}
KCMF(3:2)/rGO //LFP	40	0~4.7V	351.0~313.4 247.0~164.8 77.2~34.3	0.6~1.1 2.1~3.9 6.3~11.2	63%/250/2A g^{-1} 51%/500/2A g^{-1} 22%/1000/2A g^{-1}
	-20		115.7~65.4 37.3~21.3~8.7	0.5~1.0 1.9~3.2~5.7	95%/1000/2A g^{-1} 93%/2000/2A g^{-1} 90%/3000/2A g^{-1} 90%/5000/2A g^{-1}
KCMF(3:2)/rGO //AC/LFP(1:3)	40	0~4.4V	262.5~221.4 189.3~146.5 103.3~72.5	0.4~0.8 1.6~3.1 5.7~10.9	77%/250/2A g^{-1} 66%/500/2A g^{-1} 45%/1000/2A g^{-1}
	-20		41.0~25.1 17.3~9.6~4.6	0.3~0.7 1.4~2.6~5.5	63%/1000/2A g^{-1} 61%/2000/2A g^{-1} 58%/3000/2A g^{-1} 58%/5000/2A g^{-1}

Supplemental references

1. Q. L. Xu, R. Ding, W. Shi, D. F. Ying, Y. F. Huang, T. Yan, P. Gao, X. J. Sun and E. H. Liu, *J. Mater. Chem. A*, 2019, **7**, 8315-8326.
2. W. Shi, R. Ding, Q. L. Xu, T. Yan, Y. X. Huang, C. N. Tan, X. J. Sun, P. Gao and E. H. Liu, *Chem. Commun.*, 2019, **55**, 6739-6742.
3. L. F. Shen, H. F. Lv, S. Q. Chen, P. Kopold, P. A. van Aken, X. J. Wu, J. Maier and Y. Yu, *Adv. Mater.*, 2017, **29**, 1700142.
4. X. F. Wang and G. Z. Shen, *Nano Energy*, 2015, **15**, 104-115.
5. H. W. Wang, C. Guan, X. F. Wang, and H. J. Fan, *Small*, 2015, **11**, 1470-1477.
6. N. Arun, A. Jain, V. Aravindan, S. Jayaraman, W. C. Ling, M. P. Srinivasan and S. Madhavi, *Nano Energy*, 2015, **12**, 69-75.
7. F. X. Wang, C. Wang, Y. J. Zhao, Z. C. Liu, Z. Chang, L. J. Fu, Y. S. Zhu, Y. P. Wu and D. Y. Zhao, *Small*, 2016, **12**, 6207-6213.
8. L. W. Ji, H. H. Zheng, A. Ismach, Z. K. Tan, S. D. Xun, E. Lin, V. Battaglia, V. Srinivasan and Y. G. Zhang, *Nano Energy*, 2012, **1**, 164-171.
9. G. N. Zhu, L. Chen, Y. G. Wang, C. X. Wang, R. C. Che and Y. Y. Xia, *Adv. Funct. Mater.*, 2013, **23**, 640-647.
10. J. Hassoun, K. S. Lee, Y. K. Sun and B. Scrosati, *J. Am. Chem. Soc.*, 2011, **133**, 3139-3143.
11. Z. Moorhead-Rosenberg, E. Allcorn and A. Manthiram, *Chem. Mater.*, 2014, **26**, 5905-5913.
12. C. Wang, L. X. Wu, H. Wang, W. H. Zuo, Y. Y. Li and J. P. Liu, *Adv. Funct. Mater.*, 2015, **25**, 3524-3533.